Effect of predeformation on the propagation of vector solitons in flexible mechanical metamaterials

B. Deng, V. Tournat, and K. Bertoldi

Phys. Rev. E **98**, 053001 — Published 5 November 2018

DOI: 10.1103/PhysRevE.98.053001

Effect of pre-deformation on the propagation of vector solitons in flexible mechanical metamaterials

B. Deng,[1] V. Tournat,[1,2] and K. Bertoldi[1,3]

[1]*Harvard John A. Paulson School of Engineering and Applied Science, Harvard University, Cambridge, MA 02138*
[2]*LAUM, CNRS, Le Mans Université, Av. O. Messiaen, 72085 Le Mans, France*
[3]*Kavli Institute, Harvard University, Cambridge, MA 02138*

(Dated: October 15, 2018)

We investigate the effects of large pre-deformation on the propagation of planar solitary waves in flexible mechanical metamaterials comprising an array of hinged rotating squares. The predictive framework of our theoretical analysis shows that the pre-deformation can be exploited to control the characteristics of the supported elastic vector solitons via the tuning of the metamaterial dispersive and nonlinear properties. Together with numerical tests, our study provides a better understanding of the tunable dynamic response of flexible nonlinear mechanical metamaterials and explores more advanced configurations and effects that could open avenues for the design of systems with enhanced tunability.

I. INTRODUCTION

Artificially structured materials designed to achieve mechanical properties and functionalities that surpass those of the constituent materials (also referred to as mechanical metamaterials) are opening new avenues to manipulate motions, stresses and mechanical energy [1–3]. Such systems are also enabling control of the propagation of mechanical waves in unprecedented ways [4, 5], facilitating a wide range of applications such as wave guiding [6, 7], cloaking [8], noise reduction [9–11] and vibration control [12, 13]. However, most of mechanical metamaterials proposed to date focus on small-amplitude elastic waves and are characterized by a passive response (i.e. they operate in fixed ranges of frequencies that are impractical to tune and control after the assembly) [4, 5, 14–18].

Recent studies indicate that elastic instabilities and large deformations provide an opportunity to alter in situ the dynamic response of mechanical metamaterials. Specifically, they have shown that the width and position of their spectral gaps in frequency can be tuned and even switched on and off by varying the amount of applied deformation [19–25]. While these initial efforts have focused on linear stress waves, more recently it has also been shown that mechanical metamaterials comprising arrays of rigid units connected by thin and highly deformable ligaments support the propagation of elastic vector solitons with two components - one translational and one rotational - that are coupled together and copropagate without dispersion [26, 27].

Here, we focus on a metamaterial comprising an array of counter-rotating hinged squares [26, 28–31] that expands infinitely in transverse direction and investigate via a combination of theoretical analysis and numerical simulations the effect of large pre-deformation on nonlinear planar waves that propagate along one of its principal directions of symmetry (i.e. one of the two directions of periodicity of the structure). Our results indicate that large deformations and elastic instability can be exploited to effectively tune the width and velocity of the propagating solitary waves and even control the type of solitons supported by the system. The analyses performed in this study offer a better understanding of the dynamic response of nonlinear mechanical metamaterials and provide guidelines for the design of structures with optimized properties and enhanced tunability.

II. GEOMETRY

In this study we focus on a flexible mechanical metamaterial comprising an array of identical squares with diagonal $2l$ connected at their vertices via thin ligaments of width t (here we consider $t/(2l) \in [0.005, 0.2]$), which act as hinges (see Fig. 1-a). Two different initial configurations are considered: (i) one in which the diagonals of all the squares are aligned (without loss of generality, here we assume that they are aligned along the vertical/horizontal direction) and define square holes (see Fig. 1-a) and (ii) another one in which the neighboring squares are alternatively rotated by θ_0 in clockwise and counter-clockwise direction and define an array of diamond holes with angles $\pi/2 \pm 2\theta_0$ (see Fig. 1-b). While for the metamaterial with all diagonals aligned (for which $\theta_0 = 0$) the energy cost to rotate any square in clockwise and counter-clockwise directions is identical, the case $\theta_0 \neq 0$ introduces a disparity between the two directions of rotation. For a square rotated by θ_0 in clockwise direction it is energetically more favorable to rotate in clockwise direction under compressive loadings and in counter-clockwise direction when the system is stretched.

III. GOVERNING EQUATIONS

Since for this metamaterial the deformation localizes at the thin ligaments [26, 31], we consider the squares to be rigid. Moreover, since in this study we focus on planar waves propagating in x-direction (so that we do not expect any motion in transverse direction), we assign two degrees of freedom to each rigid unit: the displacement in the x-direction, u, and the rotation around the z-axis, θ. Moreover, to facilitate the analysis, we define the positive direction of rotation alternatively for neighboring squares. Specifically, for each square we assume the energetically favorable direction of rotation under compression to be the positive one. As such, for the $[i,\, j]$-th unit (which is rotated by θ_0 in clockwise direction - see Fig. 1-c) a clockwise rotation is positive (see blue arrow in Fig. 1-c), while for the $[i-1,\, j]$-th, $[i+1,\, j]$-th, $[i,\, j-1]$-th and $[i,\, j+1]$-th ones (which are rotated by θ_0 in counter-clockwise direction - see Fig. 1-c), counterclockwise rotations are considered positive (see purple arrow in Fig. 1-c).

As for the hinges, we model them using a combination of three linear springs: (i) their longitudinal response is captured by a spring with stiffness k_l; (ii) their shearing is governed by a spring with stiffness k_s; (iii) their bending is captured by a torsional spring with stiffness k_θ. To determine k_l, k_s and k_θ we simulate via Finite Element analyses the response of two squares connected by one ligament under three sets of boundary conditions (see Appendix A for details) [31]. We find that for a structure made of an elastic material with Poisson's ratio $\nu = 0.3$ the dimensionless stiffness $K_s = k_s/k_l$ remains almost constant over the entire range of considered ligament widths ($K_s \approx 0.5$ - see blue markers in Fig. 2). Differently, the normalized stiffness $K_\theta = k_\theta/(k_l l^2)$ is more sensitive to the ligament width and monotonically decreases as $t/(2l)$ increases (see magenta markers in Fig. 2). Moreover, our analyses also indicate that the effect of θ_0 on the spring stiffness is negligible. While the results reported in Fig. 2 are for a structure with $\theta_0 = 0$, almost identical values are found for $\theta_0 \in [0, 0.25]$. Finally, we note that all results reported in this paper are for a structure with hinges characterized by $t/(2l) = 0.05$, for which $K_s = 0.53$, $K_\theta = 0.0041$. However, qualitatively identical dynamic response is found for the entire range of considered ligament widths.

Under the assumptions listed above, the equations of motion for the $[i,\, j]$-th square are given by

$$\begin{aligned} m^{[i,\,j]}\ddot{u}^{[i,\,j]} &= \sum_{p=1}^{4} F_p^{x\;[i,\,j]}, \\ J^{[i,\,j]}\ddot{\theta}^{[i,\,j]} &= \sum_{p=1}^{4} M_p^{\;[i,\,j]}, \end{aligned} \tag{1}$$

where $m^{[i,\,j]}$ and $J^{[i,\,j]}$ are the mass and moment of inertia of the $[i,\, j]$-th rigid unit, respectively. Moreover, $F_p^{x\;[i,\,j]}$ is the force in x-direction generated at the p-th vertex of the $[i,\, j]$-th unit by the springs and $M_p^{[i,\,j]}$ represents the corresponding moment. Considering the most general case of a square initially rotated by an angle θ_0, these forces and moments are given by

$$\begin{aligned} F_p^{x\;[i,\,j]} &= \mathbf{k}_p \cdot \mathbf{\Delta l}_p^{[i,\,j]} \cdot \mathbf{e}_x, \\ M_p^{\;[i,\,j]} &= -k_\theta \Delta\theta_p^{[i,\,j]} - \left\| \mathbf{r}_p^{[i,\,j]}(\theta^{[i,\,j]}) \times \left(\mathbf{k}_p \cdot \mathbf{\Delta l}_p^{\;[i,\,j]} \right) \right\|, \end{aligned} \tag{2}$$

with

$$\mathbf{k}_p = \begin{bmatrix} k_l & 0 \\ 0 & k_s \end{bmatrix}, \quad \text{for } p = 1, 3, \tag{3}$$

and

$$\mathbf{k}_p = \begin{bmatrix} k_s & 0 \\ 0 & k_l \end{bmatrix}, \quad \text{for } p = 2, 4. \tag{4}$$

Furthermore, $\Delta\theta_p^{[i,\,j]}$ is the change in angle experienced by the rotational spring connected to the p-th vertex of the $[i,\, j]$-th rigid unit

$$\begin{aligned} \Delta\theta_1^{[i,\,j]} &= \theta^{[i,\,j]} + \theta^{[i,\,j+1]}, \\ \Delta\theta_2^{[i,\,j]} &= \theta^{[i,\,j]} + \theta^{[i+1,\,j]}, \\ \Delta\theta_3^{[i,\,j]} &= \theta^{[i,\,j]} + \theta^{[i,\,j-1]}, \\ \Delta\theta_4^{[i,\,j]} &= \theta^{[i,\,j]} + \theta^{[i-1,\,j]}, \end{aligned} \tag{5}$$

and $\mathbf{r}_p^{[i,\,j]}$ denotes the vector that connects the center of the $[i,\, j]$-th rigid unit to its p-th vertex (see Fig. 1-c)

$$\begin{aligned} \mathbf{r}_1^{[i,\,j]}(\theta^{[i,\,j]}) &= l\left[\mathcal{C}(\theta^{[i,\,j]}),\, (-1)^{i+j}\mathcal{S}(\theta^{[i,\,j]})\right], \\ \mathbf{r}_2^{[i,\,j]}(\theta^{[i,\,j]}) &= l\left[-(-1)^{i+j}\mathcal{S}(\theta^{[i,\,j]}),\, \mathcal{C}(\theta^{[i,\,j]})\right], \\ \mathbf{r}_3^{[i,\,j]}(\theta^{[i,\,j]}) &= -l\left[\mathcal{C}(\theta^{[i,\,j]}),\, (-1)^{i+j}\mathcal{S}(\theta^{[i,\,j]})\right], \\ \mathbf{r}_4^{[i,\,j]}(\theta^{[i,\,j]}) &= l\left[(-1)^{i+j}\mathcal{S}(\theta^{[i,\,j]}),\, -\mathcal{C}(\theta^{[i,\,j]})\right], \end{aligned} \tag{6}$$

with

$$\mathcal{C}(\theta^{[i,\,j]}) = \cos\left(\theta^{[i,\,j]} + \theta_0\right),\; \mathcal{S}(\theta^{[i,\,j]}) = \sin\left(\theta^{[i,\,j]} + \theta_0\right). \tag{7}$$

Finally, $\mathbf{\Delta l}_p^{[i,\,j]}$ is a vector whose entries provide the change in length along the x- and y- directions of the linear springs connected to the p-th vertex,

$$\begin{aligned} \mathbf{\Delta l}_1^{[i,\,j]} &= \left(u^{[i,\,j+1]} - u^{[i,\,j]}\right)\mathbf{e}_x + \mathbf{\Delta r}_3^{[i,\,j+1]} - \mathbf{\Delta r}_1^{[i,\,j]}, \\ \mathbf{\Delta l}_2^{[i,\,j]} &= \mathbf{\Delta r}_4^{[i+1,\,j]} - \mathbf{\Delta r}_2^{[i,\,j]}, \\ \mathbf{\Delta l}_3^{[i,\,j]} &= \left(u^{[i,\,j-1]} - u^{[i,\,j]}\right)\mathbf{e}_x + \mathbf{\Delta r}_1^{[i,\,j-1]} - \mathbf{\Delta r}_3^{[i,\,j]}, \\ \mathbf{\Delta l}_4^{[i,\,j]} &= \mathbf{\Delta r}_2^{[i-1,\,j]} - \mathbf{\Delta r}_4^{[i,\,j]}, \end{aligned} \tag{8}$$

with

$$\mathbf{\Delta r}_p^{[i,\,j]} = \mathbf{r}_p^{[i,\,j]}(\theta^{[i,\,j]}) - \mathbf{r}_p^{[i,\,j]}(0). \tag{9}$$

Note that in deriving Eqs. (8) we assume that

$$u^{[i,\,j]} = u^{[i+1,\,j]} \text{ and } \theta^{[i,\,j]} = \theta^{[i+1,\,j]} \;\forall i,\, j \tag{10}$$

since for planar waves propagating along the x-direction (as those considered in this study) we expect the deformation to be homogeneous along the y-direction.

Next, we introduce the normalized displacements $U^{[i,\,j]} = u^{[i,\,j]}/(2l\cos\theta_0)$, time $T = t\sqrt{k/m}$, stiffnesses $K_\theta = k_\theta/(k_l l^2)$ and $K_s = k_s/k_l$ and inertia $\alpha = l\sqrt{m/J}$ and rewrite Eqs. (1) in dimensionless form as

$$\begin{aligned}\frac{\partial^2 U^{[i,\,j]}}{\partial T^2} =& \sum_{p=1}^{4} \mathbf{K}_p \cdot \mathbf{\Delta L}_p^{[i,\,j]} \cdot \mathbf{e}_x \\ \frac{\partial^2 \theta^{[i,\,j]}}{\partial T^2} =& -\alpha^2 \sum_{p=1}^{4} \left[4\cos^2\theta_0 \left\| \mathbf{R}_p^{[i,\,j]} \times \left(\mathbf{K}_p \cdot \mathbf{\Delta L}_p^{[i,\,j]} \right) \right\| \right. \\ & \left. + K_\theta \Delta\theta_p^{[i,\,j]} \right],\end{aligned} \tag{11}$$

where $\mathbf{R}_p^{[i,\,j]} = \mathbf{r}_p^{[i,\,j]}/(2l\cos\theta_0)$, $\mathbf{\Delta L}_p^{[i,\,j]} = \mathbf{\Delta l}_p^{[i,\,j]}/(2l\cos\theta_0)$ and

$$\mathbf{K}_p = \begin{bmatrix} 1 & 0 \\ 0 & K_s \end{bmatrix}, \quad \text{for } p = 1, 3, \tag{12}$$

and

$$\mathbf{K}_p = \begin{bmatrix} K_s & 0 \\ 0 & 1 \end{bmatrix}, \quad \text{for } p = 2, 4. \tag{13}$$

In the following Sections we first study in detail the response of a system subjected to quasi-static unidirectional deformation in x-direction and then investigate the propagation of nonlinear planar waves along the same direction in the statically pre-deformed structure.

IV. STATIC BEHAVIOR

We start by investigating the static response of the considered metamaterial when subjected to an homogeneous strain ϵ_{st}^{xx} in x-direction, while preventing deformation in y-direction. For such loading condition
(i) the inertia terms can be neglected,

$$\frac{\partial^2 U^{[i,\,j]}}{\partial T^2} = \frac{\partial^2 \theta^{[i,\,j]}}{\partial T^2} = 0, \quad \forall\; i,\; j \tag{14}$$

(ii) the deformation is homogeneous,

$$\begin{aligned} U^{[i,\,j+1]} - U^{[i,\,j]} &= \epsilon_{st}^{xx}, \\ \theta^{[i,\,j]} &= \theta_{st}, \quad \forall\; i,\; j. \end{aligned} \tag{15}$$

where θ_{st} is the angle by which all squares rotate (with neighboring units rotating in opposite direction) due to the applied static deformation.

By substituting Eqs. (14)-(15) into Eqs. (11), we find that the only non-vanishing equation is

$$\begin{aligned} -8K_\theta\theta_{st} - \sin\Theta\,[4\epsilon_{st}^{xx}\cos\theta_0 \\ +8\,(\cos\theta_0 - \cos\Theta)] = 0, \end{aligned} \tag{16}$$

with $\Theta = \theta_0 + \theta_{st}$ (note that in our system contact between neighboring squares imposes $|\Theta| < \pi/4$). Since Eq. (16) does not admit an analytical solution, we solve it numerically to obtain the relation between the applied strain ϵ_{st}^{xx} and the resulting rotation of the squares θ_{st}. We find that for the case $\theta_0 = 0$ Eq. (16) possesses two solutions and a bifurcation point at ϵ_{cr}^{xx} (see green lines in Fig. 3-a). When loaded starting from the undeformed configuration (i.e. from $\epsilon_{cr}^{xx} = 0$ and $\theta_{st} = 0$), the squares initially only translate and do not rotate (i.e. $\theta_{st} = 0$). However, for large enough applied compressive strains the solution bifurcates, the initial branch $\theta_{st} = 0$ becomes unstable, so that the squares move to the second branch and start to rotate. Note that a given unit has equal probability to rotate in clockwise or counterclockwise direction, but its direction of rotation determines that of all the other squares (since neighboring units rotate in opposite direction). As for the critical strain $\epsilon_{st,\,cr}^{xx}$, it can be determined from Eq. (16) by setting $\theta_0 = 0$ and assuming $\theta_{st} \ll 1$, so that $\sin\theta_{st} \approx \theta_{st}$ and $\cos\theta_{st} \approx 1 - \theta_{st}^2/2$. Under these assumptions Eq. (16) reduces to

$$\theta_{st}^3 + (\epsilon_{st}^{xx} + 2K_\theta)\,\theta_{st} = 0, \tag{17}$$

from which we obtain

$$\epsilon_{st,\,cr}^{xx} = -2K_\theta, \tag{18}$$

since only for $\epsilon_{st}^{xx} < -2K_\theta$ Eq. (17) admits a solution different from $\theta_{st} = 0$.

Next, we focus on metamaterials characterized by $\theta_0 \neq 0$. Also in this case Eq. (16) possesses two distinct solutions, but there is no bifurcation point since they are disconnected (see blue and red lines in Fig. 3-a). As such, when loaded starting from the undeformed configuration, the squares immediately start to rotate and the amount of rotation monotonically increases with the applied deformation. Note that in this case the direction of rotation is dictated by the direction by which the units are rotated in the initial configuration. Squares rotated by θ_0 in clockwise direction rotate by θ_{st} in counterclockwise direction if $\epsilon_{st}^{xx} > 0$ (i.e. $\theta_{st} < 0$ if $\epsilon_{st}^{xx} > 0$) and in clockwise direction if $\epsilon_{st}^{xx} < 0$ (i.e. $\theta_{st} > 0$ if $\epsilon_{st}^{xx} < 0$). Differently, squares rotated by θ_0 in counterclockwise direction rotate by θ_{st} in clockwise direction if $\epsilon_{st}^{xx} > 0$ and in counterclockwise direction if $\epsilon_{st}^{xx} < 0$. As for the second equilibrium branch, it emerges for large enough values of the applied compressive strain and it is associated to energetically unfavorable rotations. However, since it is disconnected from the main branch, it cannot be reached by simply compressing the structure from the undeformed configuration.

Finally, the normalized stress Σ_{st}^{xx} generated by the applied deformation ϵ_{st}^{xx} is given by

$$\Sigma_{st}^{xx} = \frac{F_1^{x\ [i,j]}}{k_l 2l\cos\theta_0} = \epsilon_{st}^{xx}\cos\theta_0 + \cos\theta_0 - \cos\Theta. \tag{19}$$

As shown in Fig. 3-b, for the metamaterial with $\theta_0 = 0$ the stress-strain curve is bilinear, with a point of discontinuity at $\epsilon_{st,\,cr}^{xx} = -2K_\theta$. Differently, the stress-strain curves of the metamaterials with $\theta_0 \neq 0$ are continuous and nonlinear.

V. PROPAGATION OF PLANAR NONLINEAR WAVES IN THE PRE-DEFORMED METAMATERIAL

Having understood the static behavior of the system, we now investigate how planar nonlinear waves propagate in the pre-deformed metamaterial. In such case the total normalized displacement and rotation experienced by the $[i,\,j]$-th square can be written as

$$\begin{aligned} U^{[i,\,j]} &= U_{st}^{[i,\,j]} + U_{w}^{[i,\,j]}, \\ \theta^{[i,\,j]} &= \theta_{st}^{[i,\,j]} + \theta_{w}^{[i,\,j]}, \end{aligned} \tag{20}$$

where $U_{st}^{[i,\,j]}$ and $\theta_{st}^{[i,\,j]}$ are the displacements and rotation induced by the static pre-deformation and $U_{w}^{[i,\,j]}$ and $\theta_{w}^{[i,\,j]}$ are those generated by the propagating nonlinear wave. For quasi-static pre-deformation considered in this study $U_{st}^{[i,\,j]}$ and $\theta_{st}^{[i,\,j]}$ satisfy Eqs. (14)-(15). Moreover, as in Eqs. (10), since we consider planar waves propagating along the x-direction, we expect that

$$U_{w}^{[i+1,\,j]} = U_{w}^{[i,\,j]} \quad \text{and} \quad \theta_{w}^{[i,\,j]} = \theta_{w}^{[i+1,\,j]} \quad \forall\, i,\, j. \tag{21}$$

Substitution of Eqs. (14)-(15) and (20)-(21) into Eqs. (11) yields

$$\begin{aligned} &\frac{\partial^2 U_w^{[i,\,j]}}{\partial T^2} = U_w^{[i,\,j+1]} - 2U_w^{[i,\,j]} + U_w^{[i,\,j-1]} + \\ &- \frac{\cos(\theta_w^{[i,\,j+1]} + \Theta) - \cos(\theta_w^{[i,\,j-1]} + \Theta)}{2\cos\theta_0}, \\ &\frac{1}{\alpha^2}\frac{\partial^2 \theta_w^{[i,\,j]}}{\partial T^2} = -K_\theta\left[\theta_w^{[i,\,j+1]} + 6\theta_w^{[i,\,j]} + \theta_w^{[i,\,j-1]} + 8\theta_{st}\right] + \\ &+ K_s\cos(\theta_w^{[i,\,j]} + \Theta)\Big[\sin(\theta_w^{[i,\,j+1]} + \Theta) \\ &+ \sin(\theta_w^{[i,\,j-1]} + \Theta) - 2\sin(\theta_w^{[i,\,j]} + \Theta)\Big] + \\ &- \sin({\theta_w}^{[i,\,j]} + \Theta)\Big[2\cos\theta_0\left(U_w^{[i,\,j+1]} - U_w^{[i,\,j-1]} + 2\epsilon_{st}^{xx}\right) \\ &+ 8\cos\theta_0 - \cos(\theta_w^{[i,\,j+1]} + \Theta) + \\ &- 6\cos(\theta_w^{[i,\,j]} + \Theta) - \cos(\theta_w^{[i,\,j-1]} + \Theta)\Big]. \end{aligned} \tag{22}$$

Note that two angles come into play in Eqs. (22): (i) the angle by which the squares are rotated in the statically deformed configuration, $\Theta = \theta_0 + \theta_{st}$; and (ii) the rotation induced by the propagating nonlinear planar wave, $\theta_w^{[i,\,j]}$.

While Eqs. (22) can only be solved numerically, a deeper insight into the dynamics of the metamaterial can be achieved by further simplifying them to derive analytical solutions. To this end, we first introduce two continuous functions U and θ, which interpolate the discrete variables $U_w^{[i,\,j]}$ and $\theta_w^{[i,\,j]}$. Since in Eqs. (22) only the displacements and rotations of squares in the i-th row appear (i.e. of squares located at $x_j = j\,2l\cos\theta_0$), such continuous functions only depend on the normalized time T and the dimensionless coordinate along the x-axis $X = x/(2l\cos\theta_0)$ and are defined so that

$$\begin{aligned} U\,(X = X_j,\,T) &= U_w^{[i,\,j]}(T), \\ \theta\,(X = X_j,\,T) &= \theta_w^{[i,\,j]}(T), \end{aligned} \tag{23}$$

with

$$X_j = \frac{x_j}{2l\cos\theta_0} = \frac{j\,2l\cos\theta_0}{2l\cos\theta_0} = j. \tag{24}$$

Assuming that the width of the propagating waves is much larger than the unit cell, the displacement U and rotation θ in correspondence to the $[i,\,j-1]$-th and $[i,\,j+1]$-th units can then be expressed using Taylor expansion as

$$\begin{aligned} U\,(X_{j-1},T) &\approx U\Big|_{X_j,\,T} - \frac{\partial U}{\partial X}\Big|_{X_j,\,T} + \frac{1}{2}\frac{\partial^2 U}{\partial X^2}\Big|_{X_j,\,T}, \\ U\,(X_{j+1},T) &\approx U\Big|_{X_j,\,T} + \frac{\partial U}{\partial X}\Big|_{X_j,\,T} + \frac{1}{2}\frac{\partial^2 U}{\partial X^2}\Big|_{X_j,\,T}, \\ \theta\,(X_{j-1},T) &\approx \theta\Big|_{X_j,\,T} - \frac{\partial \theta}{\partial X}\Big|_{X_j,\,T} + \frac{1}{2}\frac{\partial^2 \theta}{\partial X^2}\Big|_{X_j,\,T}, \\ \theta\,(X_{j+1},T) &\approx \theta\Big|_{X_j,\,T} + \frac{\partial \theta}{\partial X}\Big|_{X_j,\,T} + \frac{1}{2}\frac{\partial^2 \theta}{\partial X^2}\Big|_{X_j,\,T}. \end{aligned} \tag{25}$$

Substitution of (23) and (25) into Eqs. (22) yields

$$\begin{aligned} &\frac{\partial^2 U}{\partial T^2} = \frac{\partial^2 U}{\partial X^2} - \frac{1}{\cos(\theta_0)}\frac{\partial\cos(\theta+\Theta)}{\partial X}, \\ &\frac{1}{\alpha^2}\frac{\partial^2\theta}{\partial T^2} = -K_\theta\frac{\partial^2\theta}{\partial X^2} + K_s\cos(\theta+\Theta)\frac{\partial^2\sin(\theta+\Theta)}{\partial X^2} \\ &\quad + \sin(\theta+\Theta)\frac{\partial^2\cos(\theta+\Theta)}{\partial X^2} - 8K_\theta(\theta+\theta_{st}) \\ &\quad - 4\sin(\theta+\Theta)\Big[\cos\theta_0\left(\frac{\partial U}{\partial X} + \epsilon_{st}^{xx}\right) \\ &\quad + 2\cos(\theta_0) - 2\cos(\theta+\Theta)\Big]. \end{aligned} \tag{26}$$

Moreover, if we assume that $\theta \sim \Theta \ll 1$, $\sin(\Theta+\theta)$ and $\cos(\Theta+\theta)$ can be approximated as

$$\begin{aligned} \sin(\Theta+\theta) &\approx \sin\Theta + \theta\ \cos\Theta - \theta^2\frac{\sin\Theta}{2} - \theta^3\frac{\cos\Theta}{6}, \\ \cos(\Theta+\theta) &\approx \cos\Theta - \theta\ \sin\Theta - \theta^2\frac{\cos\Theta}{2} + \theta^3\frac{\sin\Theta}{6}. \end{aligned} \tag{27}$$

By substituting Eqs. (27) into Eqs. (26) and collecting up to 3rd order terms we obtain

$$
\begin{aligned}
\frac{\partial^2 U}{\partial T^2} &= \frac{\partial^2 U}{\partial X^2} + \frac{1}{\cos\theta_0}\Big[\sin\Theta + \theta\cos\Theta - \theta^2\frac{\sin\Theta}{2}\Big]\frac{\partial\theta}{\partial X},\\
\frac{1}{\alpha^2}\frac{\partial^2\theta}{\partial T^2} &= (K_s - K_\theta)\frac{\partial^2\theta}{\partial X^2} - 4\sin\Theta\cos\theta_0\frac{\partial U}{\partial X}\\
&- 4\Big[\cos\theta_0\cos\Theta\left(2+\frac{\partial U}{\partial X}+\epsilon_{st}^{xx}\right) + 2K_\theta - 2\cos(2\Theta)\Big]\theta\\
&+ 2\sin\Theta\Big[\left(2+\frac{\partial U}{\partial X}+\epsilon_{st}^{xx}\right)\cos\theta_0 - 8\cos\Theta\Big]\theta^2\\
&+ \frac{2}{3}\left[\cos\theta_0\cos\Theta\left(2+\frac{\partial U}{\partial X}+\epsilon_{st}^{xx}\right) - 8\cos(2\Theta)\right]\theta^3,
\end{aligned} \tag{28}
$$

which represent the continuum governing equations of the system. Next, we introduce the traveling wave coordinate $\zeta = X - cT$, c being the normalized pulse velocity (the physical pulse velocity is $c\,2l\cos\theta_0\sqrt{k_l/m}$), so that Eqs. (28) become

$$
\begin{aligned}
\frac{\partial^2 U}{\partial\zeta^2} &= -\frac{1}{\cos\theta_0(1-c^2)}\\
&\Big[\sin\Theta + \theta\cos\Theta - \theta^2\frac{\sin\Theta}{2}\Big]\frac{\partial\theta}{\partial\zeta},
\end{aligned} \tag{29a}
$$

$$
\begin{aligned}
\frac{1}{\beta}\frac{\partial^2\theta}{\partial\zeta^2} &= 2\sin\Theta\cos\theta_0\frac{\partial U}{\partial\zeta} + 4\Big[2K_\theta - 2\cos(2\Theta)\\
&+ \cos\theta_0\cos\Theta\left(2+\frac{\partial U}{\partial\zeta}+\epsilon_{st}^{xx}\right)\Big]\theta\\
&- 2\sin\Theta\Big[\left(2+\frac{\partial U}{\partial\zeta}+\epsilon_{st}^{xx}\right)\cos\theta_0 - 8\cos\Theta\Big]\theta^2\\
&- \frac{2}{3}\left[\cos\theta_0\cos\Theta\left(2+\frac{\partial U}{\partial\zeta}+\epsilon_{st}^{xx}\right) - 8\cos(2\Theta)\right]\theta^3,
\end{aligned} \tag{29b}
$$

with

$$
\beta = \frac{\alpha^2}{\alpha^2(K_s - K_\theta) - c^2}. \tag{30}
$$

Integration of Eq. (29a) with respect to ζ yields

$$
\frac{\partial U}{\partial\zeta} = -\frac{1}{\cos\theta_0(1-c^2)}\left[\theta\sin\Theta + \theta^2\frac{\cos\Theta}{2} - \theta^3\frac{\sin\Theta}{6}\right] + C, \tag{31}
$$

where C is the integration constant. Since in this study we focus on the propagation of waves with a finite temporal support and do not consider periodic waves, we require that

$$
\frac{\partial U}{\partial\zeta}\Big|_{\zeta\to\infty} = 0, \tag{32}
$$

from which we obtain $C = 0$. Finally, by substituting Eq. (31) into Eq. (29b) we obtain

$$
\frac{d^2\theta}{d\zeta^2} = C_1\theta + C_2\theta^2 + C_3\theta^3, \tag{33}
$$

where

$$
\begin{aligned}
C_1 =& -4\beta\Big[\frac{\sin^2\Theta}{1-c^2} + 2\cos(2\Theta) - 2K_\theta\\
&- (2+\epsilon_{st}^{xx})\cos\theta_0\cos\Theta\Big],\\
C_2 =& -2\beta\sin\Theta\Big[\frac{(8c^2-5)\cos\Theta}{1-c^2} + (2+\epsilon_{st}^{xx})\cos\theta_0\Big],\\
C_3 =& -\frac{\beta}{3}\Big[\frac{(16c^2-9)\cos(2\Theta)-1}{1-c^2}\\
&+ 2(2+\epsilon_{st}^{xx})\cos\theta_0\cos\Theta\Big].
\end{aligned} \tag{34}
$$

Eq. (33) is the Klein-Gordon equation with quadratic and cubic nonlinearities [32], which, as recently shown for a mechanical metamaterial comprising an array of cross-shaped rigid units connected via thin ligaments [27], admits an analytical solution in the form of

$$
\theta = \frac{1}{D_1 \pm D_2\cosh(\zeta/W)}, \tag{35}
$$

where D_1, D_2 and W are solution parameters. Eq. (35) defines a solitary wave with characteristic width W and amplitude

$$
A = \theta(\zeta=0) = \frac{1}{D_1 \pm D_2}. \tag{36}
$$

Next, we determine D_1, D_2 and W as a function of the geometry of the system and the pulse velocity c. To this end, we substitute Eq. (35) into Eq. (33) and find that the latter is identically satisfied only if

$$
D_1 = -\frac{C_2}{3C_1}, \tag{37a}
$$

$$
D_2 = \sqrt{\frac{C_2^2}{9C_1^2} - \frac{C_3}{2C_1}}, \tag{37b}
$$

$$
W = \frac{1}{\sqrt{C_1}}, \tag{37c}
$$

where C_1, C_2 and C_3 are defined in Eqs. (34). At this point it is important to note that the existence of the two solutions defined by Eq. (35) requires that

(i) W is real valued, yielding

$$
C_1 > 0 \tag{38}
$$

(ii) D_2 is a real number, yielding

$$
\frac{C_2^2}{9C_1^2} - \frac{C_3}{2C_1} > 0 \tag{39}
$$

(iii) the denominator in Eq. (35) is different from zero,

$$
D_1 \pm D_2\cosh(\zeta/W) \neq 0. \tag{40}
$$

Violation of Eqs. (38)-(40) may result in the formation of amplitude gaps for the solitary waves (i.e. ranges in amplitude where elastic soliton propagation is forbidden) [27]. Moreover, since $D_2 > 0$ (see Eq. (37b)) and $\cosh(\zeta/W) \in [1, \infty)$, Eq. (40) is only satisfied if $|D_1| < D_2$. Differently, for $|D_1| > D_2$ only one of the two solitary waves defined by Eq. (35) exists. Specifically, if the system parameters for a metamaterial with $\theta_0 \geq 0$ (for which D_1 is always smaller than D_2) are such that $-D_1 > D_2$, the solution given by Eq. (35) reduces to

$$\theta = \frac{1}{D_1 - \ D_2 \cosh\left(\zeta/W\right)}. \tag{41}$$

Further, it is important to point out that for $D_2 = 0$ the solution given by Eq. (35) reduces to a constant (i.e. $\theta = 1/D_1$ when $D_2 = 0$). Notably, we find that for $D_2 = 0$, (i.e. $2C_2^2 - 9C_1C_3 = 0$) Eq. (33) can be rewritten as

$$\frac{d^2\theta}{d\zeta^2} = C_3\theta\left(\theta + \frac{C_2}{3C_3}\right)\left(\theta + \frac{2C_2}{3C_3}\right), \tag{42}$$

which admits the non-trivial solution

$$\theta = \frac{A}{2}\left[1 - \tanh\left(\pm\frac{\zeta}{W}\right)\right], \tag{43}$$

with

$$A = -\frac{2C_2}{3C_3}, \tag{44a}$$

$$W = \frac{2}{\sqrt{C_1}}. \tag{44b}$$

Eqs. (43)-(44) define either a kink (in the case of + sign in Eq. (43)) or anti-kink (in the case of − sign in Eq. (43)), which are typically associated to a phase transition [33–35]. As discussed in the following Section, this solution takes the deformed metamaterial from one static equilibrium position to another one. Note that Eqs. (42) and (43) correspond to some extent to the well-known ϕ^4 model [36], with an additional topological constraint. Since Eq. (43) defines a transition between the two existing stable states, in our system a kink must necessarily be followed by an anti-kink.

Finally, the solution for the displacement U is found by integrating Eq. (31)

$$U = \int_{\zeta}^{\infty} \frac{1}{\cos\theta_0(1-c^2)}\left[\theta(\zeta')\sin\Theta + \theta(\zeta')^2\frac{\cos\Theta}{2} - \theta(\zeta')^3\frac{\sin\Theta}{6}\right]d\zeta'. \tag{45}$$

with θ given by either Eq. (35) or Eq. (41) or Eq. (43). As recently found for undeformed structures comprising a network of rigid units connected by thin and highly deformable ligaments [26, 27], Eqs. (35), (41), (43) and (45) indicate that also the pre-deformed system considered in this study supports the propagation of elastic vector solitons (i.e. solitary waves with two components - one translational and one rotational - that are coupled together and co-propagate without dispersion). Moreover, since the solution depends on ϵ_{st}^{xx}, they show that the characteristics of such solitary waves can be controlled by tuning the amount of applied deformation.

A. Metamaterials with $\theta_0 = 0$

To better understand the effect of the applied deformation on the propagation of solitary waves, we start focusing on a metamaterial with $\theta_0 = 0$ (i.e. a metamaterial in which the diagonals of all the squares are aligned). In Fig. 4 we show the solitary waves supported by the structure as a function of the applied pre-deformation ϵ_{st}^{xx}. We find that three different scenarios are possible: (i) $D_2 > 0$, so that the supported solitons are defined by Eq. (35) (pink region in Fig. 4); (ii) $D_2 = 0$, so that the supported solitons are defined by Eq. (43) (blue region in Fig. 4); (iii) at least one of the condition defined by Eqs. (38)-(40) is violated, so that no physical solution exists (grey region in Fig. 4). Those findings indicate that ϵ_{st}^{xx} can be exploited to switch between the different types of solitary waves supported by the structure. While in the pre-buckling regime (i.e. for $\epsilon_{st}^{xx} > \epsilon_{st,\ cr}^{xx}$) the metamaterial supports the propagation of vector solitons with rotational component defined by Eq. (35), in the entire post-buckling regime (i.e. for $\epsilon_{st}^{xx} < \epsilon_{st,\ cr}^{xx}$) only those with rotational component defined by Eq. (43) can propagate.

1. *Pre-buckling regime:* $\epsilon_{st}^{xx} > \epsilon_{st,\ cr}^{xx}$

Having determined that prior to buckling the metamaterials with $\theta_0 = 0$ support the propagation of the solitary waves defined by Eq. (35), we now investigate how their width W and velocity c are affected by the applied deformation. Since in a metamaterial with $\theta_0 = 0$ the squares do not rotate prior to buckling (i.e. $\theta_{st} = 0$ for $\epsilon_{st}^{xx} > \epsilon_{st,\ cr}^{xx}$), for $\epsilon_{st}^{xx} > \epsilon_{st,\ cr}^{xx}$ Eqs. (34) reduce to

$$\begin{aligned} C_1 =& 4\beta\left[2K_\theta + \epsilon_{st}^{xx}\right], \\ C_2 =& 0, \\ C_3 =& -2\beta\left[\frac{2c^2-1}{1-c^2} + \frac{\epsilon_{st}^{xx}}{3}\right], \end{aligned} \tag{46}$$

and the general solution given by Eqs. (35) and (45) simplifies to

$$\begin{cases} \theta &= A\ \mathrm{sech}\left(\dfrac{\zeta}{W}\right), \\ U &= \dfrac{A^2W}{2(1-c^2)}\left[1 - \tanh\left(\dfrac{\zeta}{W}\right)\right]. \end{cases} \tag{47}$$

Moreover, substitution of Eqs. (46) into Eqs. (36) and (37c) yields

$$\begin{aligned} W &= \frac{1}{2\alpha\sqrt{2K_\theta + \epsilon_{st}^{xx}}}\sqrt{(K_s - K_\theta)\alpha^2 - 1 + \frac{3}{\gamma + 6}}, \\ c &= \sqrt{\frac{\gamma + 3}{\gamma + 6}}, \end{aligned} \tag{48}$$

with

$$\gamma = 12A^2\left(\epsilon_{st}^{xx} + 2K_\theta\right) - \epsilon_{st}^{xx}. \tag{49}$$

Eqs. (48) clearly show that both the width and the velocity of the solitons propagating with a given amplitude A can be controlled by tuning the applied pre-deformation ϵ_{st}^{xx}. More specifically, Eqs. (48) indicate that:
(i) when the metamaterial is stretched (i.e. for $\epsilon_{st}^{xx} > 0$), the velocity c becomes larger (see Fig. 5-a) and the width W becomes smaller (see Fig. 5-b) as the amount of applied pre-strain ϵ_{st}^{xx} is increased;
(ii) upon compression (i.e. for $\epsilon_{st}^{xx} < 0$), c progressively decreases (see Fig. 5-a), while W increases (see Fig. 5-b). It is also important to note that W approaches infinity at the onset of buckling (i.e. $W \to \infty$ at $\epsilon_{st}^{xx} = \epsilon_{st}^{xx,\,cr} = -2K_\theta$ - see Fig. 5-b). This further confirms that at the onset of buckling the considered metamaterial cannot support anymore the propagation of the elastic vector solitons defined by Eqs. (47).

To validate the predictions of our continuum model, we numerically solve the system of ODEs given by Eqs. (22). In our numerical analysis we consider a chain comprising 1×500 squares, implement periodic boundary conditions in the transverse direction and apply the theoretical solution given by Eq. (47) to the first square of the chain (while leaving the other end free). In Fig. 6 we compare analytically (lines) and numerically (markers) predicted rotations (left) and normalized displacements (right) profiles at different level of applied deformation ϵ_{st}^{xx}, assuming $A = 0.30$. In general, we observe an excellent agreement between the numerical results and the predictions of our continuum model. The numerical simulations confirm that in the postbuckling regime the considered metamaterial cannot support the solitons defined by Eq. (47), as the wave is dispersed during propagation if $\epsilon_{st}^{xx} < \epsilon_{st,\,cr}^{xx}$ (see results for $\epsilon_{st}^{xx} = -0.018$ in Fig. 6-c). Moreover, they also indicate that solitary waves are not supported by the system for large enough positive ϵ_{st}^{xx} (see results for $\epsilon_{st}^{xx} = 0.012$ in Fig. 6-e). This is because for large enough applied tensile deformations the width W of the propagating solitons is so small that the continuum approximation introduced to derive our analytical solution (Eqs. (25)) is not anymore valid. To better characterize this effect, in Fig. 6-f we report the number of units after which the amplitude of the solitary wave is reduced by half, $N_{0.5A}$. The contour plot shows that $N_{0.5A}$ significantly drops when ϵ_{st}^{xx} and A are such that $W \sim 2$. Therefore, our numerical results indicate that, although the considered discrete system does not exhibit amplitude gaps for elastic vector solitons [27] (since W is real-valued for any amplitude A - see Fig. 5-b), it still does not support the propagation of solitary waves if W is small enough (albeit greater than zero).

2. *Post-buckling regime:* $\epsilon_{st}^{xx} < \epsilon_{st,\,cr}^{xx}$

Next, we turn our attention to the post-buckling regime, where only vector solitons with rotational component defined by Eq. (43) can propagate (see Fig. 4). In Fig. 7 we report the evolution of the amplitude A and width W of such solitons (given by Eqs. (44)) as a function of c and ϵ_{st}^{xx}. We find that the width W monotonically decreases as the applied pre-compression is increased (see Fig. 7-a). Hovewer, while in the subsonic regime (i.e. for $c < 1$) W remains large enough (i.e. $\min(W) = 6.68$ for the considered range of applied strain) so that we do not expect discrete effects to prevent the propagation of the solitons, we find that the supersonic solitons (i.e. solitons with $c > 1$) are characterized by a very small width (i.e. $\min(W) = 0.05$ for the considered range of applied strain). As for the amplitude A, the plot in Fig. 7-b indicates that it is fully determined by ϵ_{st}^{xx} and not affected by c. To further investigate this point, we assume that the static rotations induced by buckling are small, so that

$$\sin\theta_{st} \approx \theta_{st}, \text{ and } \cos\theta_{st} \approx 1 - \frac{\theta_{st}^2}{2}. \tag{50}$$

Substitution of Eqs. (50) into Eq. (44a) yields

$$A = -\frac{2C_2}{3C_3} \approx -2\theta_{st}, \tag{51}$$

which confirms that the amplitude of the propagating solitons only depends on the amount of applied pre-deformation. Moreover, Eq. (51) indicates that the solitons take the buckled structure from one stable configuration (characterized by θ_{st}) to the mirrored one on the same equilibrium branch (characterized by $-\theta_{st}$ - see Fig. 3-a).

Next, we verify the predictions of our continuum model by comparing them to numerical results obtained by integrating the system of ODEs given by Eqs. (22) on a chain comprising 1×500 squares and with periodic boundary conditions in transverse direction. The results shown in Fig. 8 confirm that in the post-buckling regime the considered metamaterial supports the propagation of vector solitons with rotational component defined by Eq. (43). They also show that for the subsonic solitons the displacement U is negative and has a positive gradient (see Figs. 8-a and -b). As such, the solitons with $c < 1$ stretch the structure in the longitudinal direction during propagation. Note that in Fig. 8-c we show the propagation of a sequence of three kinks and anti-kinks, corresponding to the plus and minus sign solutions of Eq. (43). Differently from Sine-Gordon systems comprising an infinite number of stable states and consequently supporting arbitrary sequences of kinks or anti-kinks [36], our system has only two stable states. Consequently, a kink must necessarily be followed by an anti-kink. Since for both solutions the displacement U is negative and has a positive gradient, the train of kinks and anti-kinks leads to a cumulated stair-like displacement along the chain. As for the rotation, the square jumps back and forth between the two stable angles. Finally, in Figs. 8-d and -e we focus on the supersonic kink solitons. We find that they compress the metamaterial during propagation (see Figs. 8-d and -e). However, since their width is very small, they are supported by the discrete systems only when the applied deformation is very close to the critical strain (see Figs. 8-d and -e).

B. Metamaterials with $\theta_0 \neq 0$

While in the previous Section we have focused on the dynamic response of metamaterials with $\theta_0 = 0$, we now turn our attention to structures in which the squares are initially rotated (i.e. metamaterials with $\theta_0 \neq 0$). We start by investigating the characteristics of the solitons supported by these metamaterials as a function of the applied deformation. As shown in Fig. 9, three different scenarios are possible: (i) $|D_1| < D_2$, so that the supported solitons are defined by Eq. (35) (pink region in Fig. 9); (ii) $|D_1| > D_2$, so that the supported solitons are defined by Eq. (41) (yellow region in Fig. 9); (iii) at least one of the condition defined by Eqs. (38)-(40) is violated, so that no physical solution exists (grey region in Fig. 9). Furthermore, the results shown in Figs. 9-a and -b for structures with $\theta_0 = 0.01$ and 0.25 also indicate that θ_0 strongly affects the dynamic response of the system. The structure with $\theta_0 = 0.01$ supports subsonic vector solitons with rotational component defined by Eq. (35) for all considered values of ϵ_{st}^{xx} and supersonic solitons with θ defined by Eq. (41) only for large enough values of applied pre-compression. Differently, in the structure with $\theta_0 = 0.25$ both types of solitary waves are supported for the entire range of applied pre-deformation and also subsonic solitons with rotational component defined by Eq. (41) can propagate for large enough values of applied pre-compression. To further understand the effect of θ_0 on the propagation of solitary waves, in Fig. 10-c we focus on $\epsilon_{st}^{xx} = 0$ and investigate the types of solitons supported by our metamaterials as a function of θ_0 (note that qualitatively identical behavior is found for any considered value of ϵ_{st}^{xx}). As suggested by the results reported in Figs. 9-a and -b, we find that θ_0 strongly affects the presence of the vector solitons with θ defined by Eq. (41), since they are supported by the system only for large enough values of initial rotation of the squares.

Next, we focus on the metamaterial with $\theta_0 = 0.01$ and investigate how the velocity c and width W of the supported solitons are affected by ϵ_{st}^{xx}. Specifically, in Fig. 10-a and -b we report the evolution of c and W as a function of A and ϵ_{st}^{xx} (note that these plots are obtained by combining Eqs. (36) and (37c), which provide the A-c and W-c relations, respectively). Similarly to the structure with $\theta_0 = 0$, we find that also for this metamaterial the velocity and width of the vector solitons with rotational component defined by Eq. (35) become larger and smaller, respectively, as ϵ_{st}^{xx} increases (see Figs. 10-a and -b). However, while in the case $\theta_0 = 0$ the characteristics of the propagating solitons are not affected by the direction of the rotations that they induce (so that in Fig. 5 we only plot the solution for $A > 0$), in the system with $\theta_0 = 0.01$ there is a disparity between the two directions of rotations. A solitary wave that induces energetically favorable rotations (i.e. for which $A > 0$) travels slower than the corresponding one inducing energetically unfavorable rotations (i.e. for which $A < 0$ - see Fig. 11-a). Furthermore, the metamaterial with $\theta_0 = 0.01$ has an amplitude gap for solitons (see gray region in Fig. 10), inside which Eq. (33) has no physical solution. As shown by the numerical results reported in Fig. 11-b, if a soliton with amplitude inside the gap is excited, it cannot propagate through the system. It is important to note that such gap is highly asymmetric and only affects the solitons that induce energetically unfavorable rotations (i.e. the upper bound of the gap is $A = 0$, so that all solitons that induce energetically favorable rotations at the squares can propagate, regardless of their amplitude). Our results also indicate that the gap becomes more pronounced as the amount of applied pre-compression is increased. This is because the applied compressive strain further increases the rotation of the squares, making the asymmetry of the structure even stronger. To further explore the effect of ϵ_{st}^{xx} on the width of the gap, in Fig. 10-c we report the evolution of its lower limit, A_{lower}, as a function of the applied strain ϵ_{st}^{xx} and the hinge width $t/(2l)$ (note that for a metamaterial with $\theta_0 = 0.01$ the upper limit of the gap is always 0). We find that the gap almost vanishes as the thickness of the hinges increases and that the influence of ϵ_{st}^{xx} on A_{lower} is more pronounced for the structures with thinner hinges. Finally, we note that the supersonic vector solitons with θ defined Eq. (41) emerges as a small island inside the gap (see Figs. 10-a and -b). However, these solitons have very small width (i.e. $\max(W) = 0.68$), so that they are not supported by the discrete system (Fig. 11-c).

Finally, in Fig. 12 we focus on a structure with $\theta_0 = 0.25$. We find that by increasing the initial rotation of the squares the amplitude gap widens and becomes more pronounced over the entire range of applied deformation. As for the vector solitons with θ defined by Eq. (41), they emerge as two islands inside the gap. However, also in this case because of their small width we do not expect them to propagate in the discrete system.

VI. CONCLUSIONS

In summary, we have focused on a mechanical metamaterial comprising an array of squares connected at their vertices via thin ligaments and used numerical simulations and theoretical analysis to investigate the effect of static pre-deformation on planar solitary waves that propagate along one of its pricipal directions. Our analyses indicate that (i) the applied pre-deformation strongly affect the width and velocity of the propagating solitons; (ii) depending on the amount of applied deformation different types of solitons are supported by the system, of which we systematically studied the existence and properties; (iii) solitons with small width (i.e. $W < 2$) are not supported by the discrete system, as disperse during propagation; (iv) the width of the amplitude gaps can be tuned via the applied deformation. We believe that the results presented in this paper provide useful guidelines for the design of structures with enhanced wave tunability, and target nonlinear elastic properties. Moreover, we envision application of the observed kink waves in the reconfiguration of complex bistable structures, resulting in changes of their mechanical, thermal, acoustical properties.

ACKNOWLEDGMENTS

K.B. acknowledges support from the National Science Foundation under Grant No. DMR-1420570 and EFMA-1741685 and from the Army Research Office under Grant No. W911NF-17-1-0147.

[1] M. Kadic, T. Bückmann, R. Schittny, and M. Wegener, Reports on Progress in Physics **76**, 126501 (2013).

[2] J. Christensen, M. Kadic, O. Kraft, and M. Wegener, MRS Communications **5**, 453 (2015).

[3] V.-V. C. J. Bertoldi, K. and M. van Hecke, Nature Reviews **2**, 17066 (2017).

[4] M. Hussein, M. Leamy, and M. Ruzzene, Applied Mechanics Reviews **66**, 040802 (2014).

[5] Y. Wu, M. Yang, and P. Sheng, Journal of Applied Physics **123**, 090901 (2018).

[6] A. Khelif, A. Choujaa, S. Benchabane, B. Djafari-Rouhani, and V. Laude, Applied Physics Letters **84**, 4400 (2004).

[7] M. Kafesaki, M. M. Sigalas, and N. Garcia, Physical Review Letters **85**, 4044 (2000).

[8] S. Cummer and D. Schurig, New Journal of Physics **9**, 45 (2007).

[9] D. Elser, U. L. Andersen, A. Korn, O. Glöckl, S. Lorenz, C. Marquardt, and G. Leuchs, Physical Review Letters **97**, 133901 (2006).

[10] T. Elnady, A. Elsabbagh, W. Akl, O. Mohamady, V. M. Garcia-Chocano, D. Torrent, F. Cervera, and J. Sánchez-Dehesa, Applied Physics Letters **94**, 134104 (2009).

[11] F. Casadei, L. Dozio, M. Ruzzene, and K. Cunefare, Journal of Sound and Vibration **329**, 3632 (2010).

[12] L. Airoldi and M. Ruzzene, New Journal of Physics **13**, 113010 (2011).

[13] F. Casadei, B. Beck, K. A. Cunefare, and M. Ruzzene, International Journal of Solids and Structures **23**, 1169 (2012).

[14] V. K.K. and E. L., International Journal of Solids and Structures **19**, 393 (1983).

[15] M. Kafesaki, M. M. Sigalas, and E. N. Economou, Solid State Commun. **96**, 285 (1995).

[16] X. Zhang, Z. Liu, Y. Liu, and F. Wu, Physics Letters A **313**, 455 (2003).

[17] S. X. Yang, J. H. Page, Z. Y. Liu, M. L. Cowan, C. T. Chan, and P. Sheng, Phys. Rev. Lett. **93**, 024301 (2004).

[18] R. Sainidou, B. Djafari-Rouhani, Y. Pennec, and J. O. Vasseur, Phys. Rev. B **73**, 024302 (2006).

[19] K. Bertoldi and M. C. Boyce, Physical Review B **77**, 052105 (2008).

[20] P. Wang, J. Shim, and K. Bertoldi, Physical Review B **88**, 014304 (2013).

[21] D. Mousanezhad, S. Babaee, R. Ghosh, E. Mahdi, K. Bertoldi, and A. Vaziri, Physical Review B **92**, 104304 (2015).

[22] S. Rudykh and M. Boyce, Physical Review Letters **112**, 034301 (2014).

[23] S. Babaee, P. Wang, and K. Bertoldi, Journal of Applied Physics **117**, 244903 (2015).

[24] P. Celli, S. Gonella, V. Tajeddini, A. Muliana, S. Ahmed, and Z. Ounaies, arXiv , 1609.08404 (2016).

[25] P. Wang, F. Casadei, S. Shan, J. Weaver, and K. Bertoldi, Physical Review Letters **113**, 014301 (2014).

[26] B. Deng, J. Raney, V. Tournat, and K. Bertoldi, Physical Review Letters **118**, 204102 (2017).

[27] B. Deng, P. Wang, Q. He, V. Tournat, and K. Bertoldi, Nature Communications **9**, 3410 (2018).

[28] J. Grima and K. Evans, J. Mat. Sci. Lett. **19**, 1563 (2000).

[29] Y. Cho, J.-H. Shin, A. Costa, T. Kim, V. Kunin, J. Li, S. Yeon Lee, S. Yang, H. Han, I.-S. Choi, and D. Srolovitz, Proc. Natl. Acad. Sci. USA **111**, 17390 (2014).

[30] M. Taylor, L. Francesconi, M. Gerends, A. Shanian, C. Carson, and K. Bertoldi, Advanced Materials **26**, 2365 (2014).

[31] C. Coulais, C. Kettenis, and M. van Hecke, arXiv , 1708.04643 (2017).

[32] A. Polyanin and V. Zaitsev, Handbook of Nonlinear Partial Differential Equations (Chapman and Hall/CRC, 2011).

[33] N. Manton and P. Sutcliffe, Topological Solitons, Cambridge Monographs on Mathematical Physics (Cambridge University Press, 2004).

[34] J. R. Raney, N. Nadkarni, C. Daraio, D. M. Kochmann, J. A. Lewis, and K. Bertoldi, Proceedings of the National Academy of Sciences **113**, 9722 (2016), http://www.pnas.org/content/113/35/9722.full.pdf.

[35] B. G.-g. Chen, N. Upadhyaya, and V. Vitelli, Proceedings of the National Academy of Sciences **111**, 13004 (2014), http://www.pnas.org/content/111/36/13004.full.pdf.

[36] T. Dauxois and M. Peyrard, Physics of Solitons (Cambridge University Press, 2006).

VII. APPENDIX A: NUMERICAL SIMULATIONS TO DETERMINE k_l, k_s AND k_θ

To determine the spring stiffness k_l, k_s and k_θ as a function of the hinges geometry, we conduct Finite Element simulations using the commercial package Abaqus/Standard. In all our analysis, (i) we consider two half squares (see dark blue region in Fig. 13); (ii) we assume plane strain conditions; (iii) we mesh the models using hybrid quadratic triangular elements (Abaqus element type: CPE8H) and ascertain the accuracy of the mesh through a mesh refinement study; (iv) we use a linear material with Young's modulus $E = 1$ MPa and Poisson's ratio $\nu = 0.3$ to capture the material response; (v) we do not account for geometric non-linearities.

To determine the spring stiffness k_l and k_s we apply an horizontal displacement δ_l and a vertical displacement δ_s to the two boundaries of our model, respectively (see Figs. 13- a and -b). The stiffness is then obtained from the measured reaction force F_l and F_s (given by the sum of all reaction forces at the nodes located on one of the two boundaries) as

$$k_l = \frac{F_l}{2\delta_l}, \quad k_s = \frac{F_s}{2\delta_s}. \tag{52}$$

As for the stiffness k_θ, the two squares are rotated by applying the displacement distribution δ_t shown in Fig. 13-c. The stiffness k_θ is then obtained as

$$k_\theta = \frac{l M_t}{2\max(\delta_t)} \tag{53}$$

where M_t is calculated by summing up the moment generated by every nodal force on the boundary.

FIGURES

FIG. 1. Schematics of the mechanical metamaterial considered in this study. (a) Configuration characterized by $\theta_0 = 0$. (b) Configuration characterized by $\theta_0 \neq 0$. The details of the hinge geometry are shown in the zoom-in. (c) Discrete model based on rigid units connected at their vertices by springs.

FIG. 2. Evolution of the dimensionless stiffnesses K_s (blue markers) and K_θ (magenta markers) as a function of the normalized hinge width $t/(2l)$.

FIG. 3. (a) Rotation-strain bifurcation diagram for metamaterials with $\theta_0 = 0$ (green lines), $\theta_0 = 0.01$ (red lines) and $\theta_0 = 0.25$ (blue lines). Solid/dashed lines represent stable/unstable branches, respectively. The vertical dashed line indicates the critical strain $\epsilon^{xx}_{st,\,cr} = -2K_\theta$ (b) Evolution of the normalized stress Σ^{xx}_{st} as a function of the applied strain ϵ^{xx}_{st}. Note that both stress and strain are defined negative for compression and positive for tension.

FIG. 4. Effect of the applied strain ϵ^{xx}_{st} on the velocity c and on the types of solitary waves supported by a metamaterial with $\theta_0 = 0$. The red dashed line indicates the critical strain $\epsilon^{xx}_{st,\ cr}$.

FIG. 5. Effect of the applied strain ϵ^{xx}_{st} on the velocity c and width W of the solitons according to Eqs. (48). (a) Evolution of c as a function of A and ϵ^{xx}_{st}. (b) Evolution of c as a function of A and ϵ^{xx}_{st}. The circular markers indicate the points considered in our numerical analysis, whose results are presented in Fig. 6.

FIG. 6. (a-e) Numerical (markers) and analytical (lines) results for a metamaterial characterized by $\theta_0 = 0$ (see Movie S1 for animations). Rotation (left) and normalized displacement (right) profiles at different level of applied pre-deformation: (a) $\epsilon^{xx}_{st} = 0$, (b) $\epsilon^{xx}_{st} = -0.008$, (c) $\epsilon^{xx}_{st} = -0.018$, (d) $\epsilon^{xx}_{st} = 0.008$, (e) $\epsilon^{xx}_{st} = 0.012$. In each plot we show the profiles at $T = 1050$, 1550, and 2050. Note that the results for the buckled system (i.e. for $\epsilon^{xx}_{st} = -0.018$) are obtained by applying the solution given by Eq. (47) with $W = 6$. Although the choice of W is completely arbitrary, quantitatively identical results are obtained for any real W. (f) Number of units after which the amplitude of the solitary wave is reduced by half, $N_{0.5A}$, as a function of the applied strain ϵ^{xx}_{st} and amplitude A.

FIG. 7. Effect of the applied strain ϵ^{xx}_{st} on the width W and velocity c of solitons with rotational component defined by Eq. (43). (a) Evolution of W as a function of c and ϵ^{xx}_{st}. (b) Evolution of A as a function of c and ϵ^{xx}_{st}. The gray shaded areas highlight regions where no solution exists. The circular markers indicate the points considered in our numerical analysis, whose results are presented in Fig. 8.

FIG. 8. Numerical (markers) and analytical (lines) results for a buckled metamaterial characterized by $\theta_0 = 0$ (see Movie S1 for animations). Rotation (left) and normalized displacement (right) profiles for: (a) $\epsilon^{xx}_{st} = -0.01$ and $c = 0.4$ at $T = 480$, 800 and 1280; (b) $\epsilon^{xx}_{st} = -0.02$ and $c = 0.4$ at $T = 480$, 800 and 1280; (c) $\epsilon^{xx}_{st} = -0.02$ and $c = 0.4$ when excited with a sequence of kinks and anti-kinks; (d) $\epsilon^{xx}_{st} = -0.0085$ and $c = 1.2$ at $T = 220$, 400 and 580; (e) $\epsilon^{xx}_{st} = -0.009$ and $c = 1.2$ at $T = 460$, 580 and 700.

FIG. 9. (a)-(b) Effect of the applied strain ϵ_{st}^{xx} on the velocity c and types of solitary waves supported by a metamaterial with (a) $\theta_0 = 0.01$ and (b) $\theta_0 = 0.25$. (c) Effect of the angle θ_0 on the velocity c and types of solitary waves supported by an undeformed metamaterial (i.e. ϵ_{st}^{xx}=0).

FIG. 10. (a)-(b) Effect of the applied strain ϵ_{st}^{xx} and amplitude A on (a) the velocity c and (b) the width W of the solitons supported by a metamaterial with $\theta_0 = 0.01$. The gray region highlights the amplitude gap as predicted by the continuum model. The circular markers indicate the points considered in our numerical analysis, whose results are presented in Fig. 11. (c) Evolution of the amplitude gap's lower limit, A_{lower}, as a function of the applied strain ϵ_{st}^{xx} and the hinge width $t/(2l)$ for a metamaterial with $\theta_0 = 0.01$.

FIG. 11. Numerical (markers) and analytical (lines) results for a metamaterial characterized by $\theta_0 = 0.01$ (see Movie S1 for animations). Rotation (left) and normalized displacement (right) profiles for (a) $\epsilon_{st}^{xx} = -0.01$ and $A = \pm 0.30$ at $T =$ 250, 450 and 650; (b) $\epsilon_{st}^{xx} = -0.01$ and $A = -0.24$ at $T =$ 260, 440 and 620; (c) $\epsilon_{st}^{xx} = -0.02$ and $A = -0.19$ at $T =$ 200, 300 and 400.

FIG. 12. Effect of the applied strain ϵ_{st}^{xx} and amplitude A on (a) the velocity c and (b) the width W of the solitons supported by a metamaterial with $\theta_0 = 0.25$. The gray region highlights the amplitude gap as predicted by the continuum model.

FIG. 13. Schematics highlighting the boundary conditions used in our FE simulations to determine (a) k_l, (b) k_s and (c) k_θ.

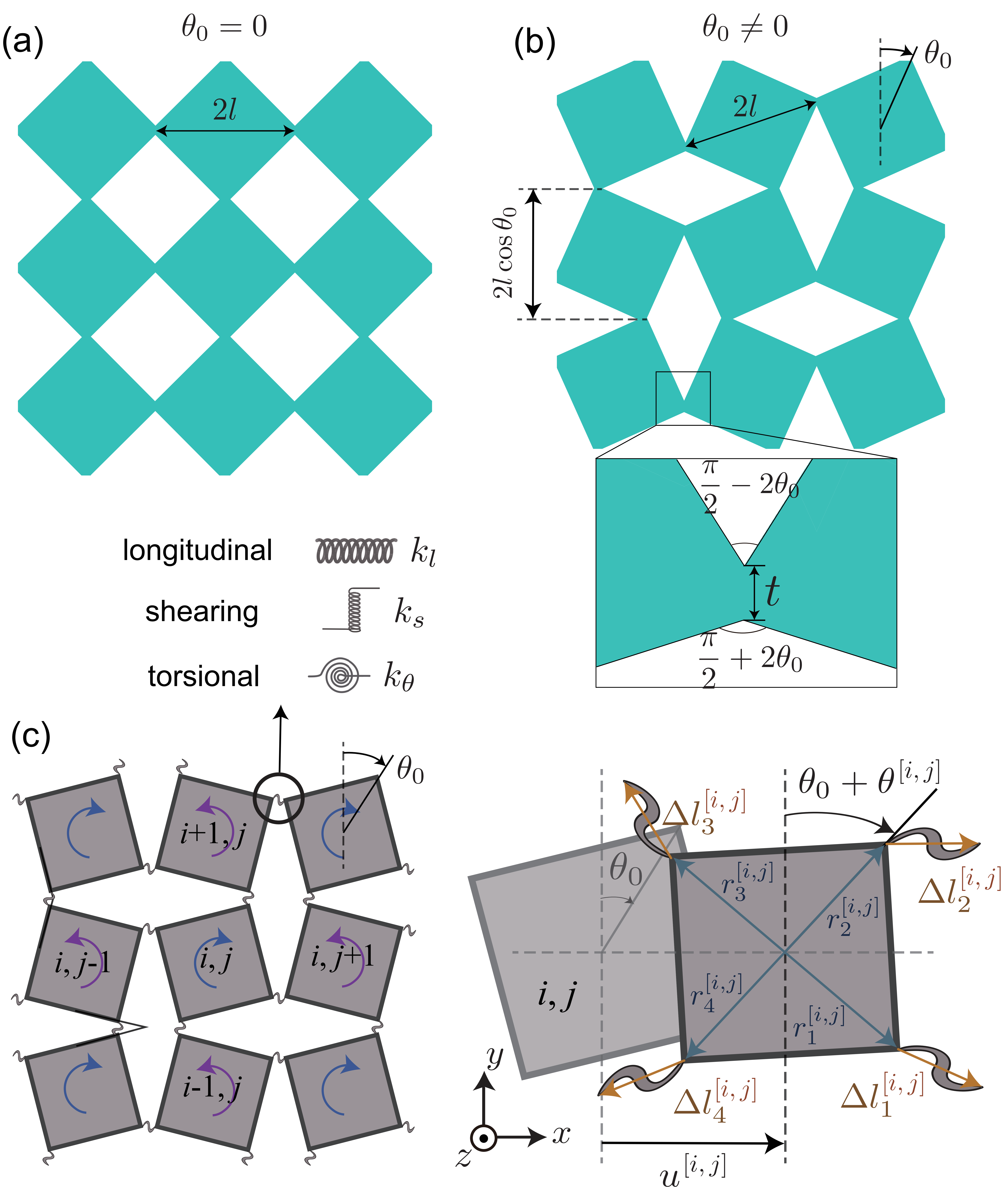

(a)
$\theta_0 = 0$
$2l$
(b)
$\theta_0 \neq 0$
θ_0
$2l$
$2l\cos\theta_0$
$\frac{\pi}{2} - 2\theta_0$
t
$\frac{\pi}{2} + 2\theta_0$
longitudinal
k_l
shearing
k_s
torsional
k_θ
(c)
θ_0
i+1,j
i,j-1
i,j
i,j+1
i-1,j
$\theta_0 + \theta^{[i,j]}$
$\Delta l_3^{[i,j]}$
$\Delta l_2^{[i,j]}$
$\Delta l_4^{[i,j]}$
$\Delta l_1^{[i,j]}$
$r_3^{[i,j]}$
$r_2^{[i,j]}$
$r_4^{[i,j]}$
$r_1^{[i,j]}$
θ_0
i,j
x
y
z
$u^{[i,j]}$

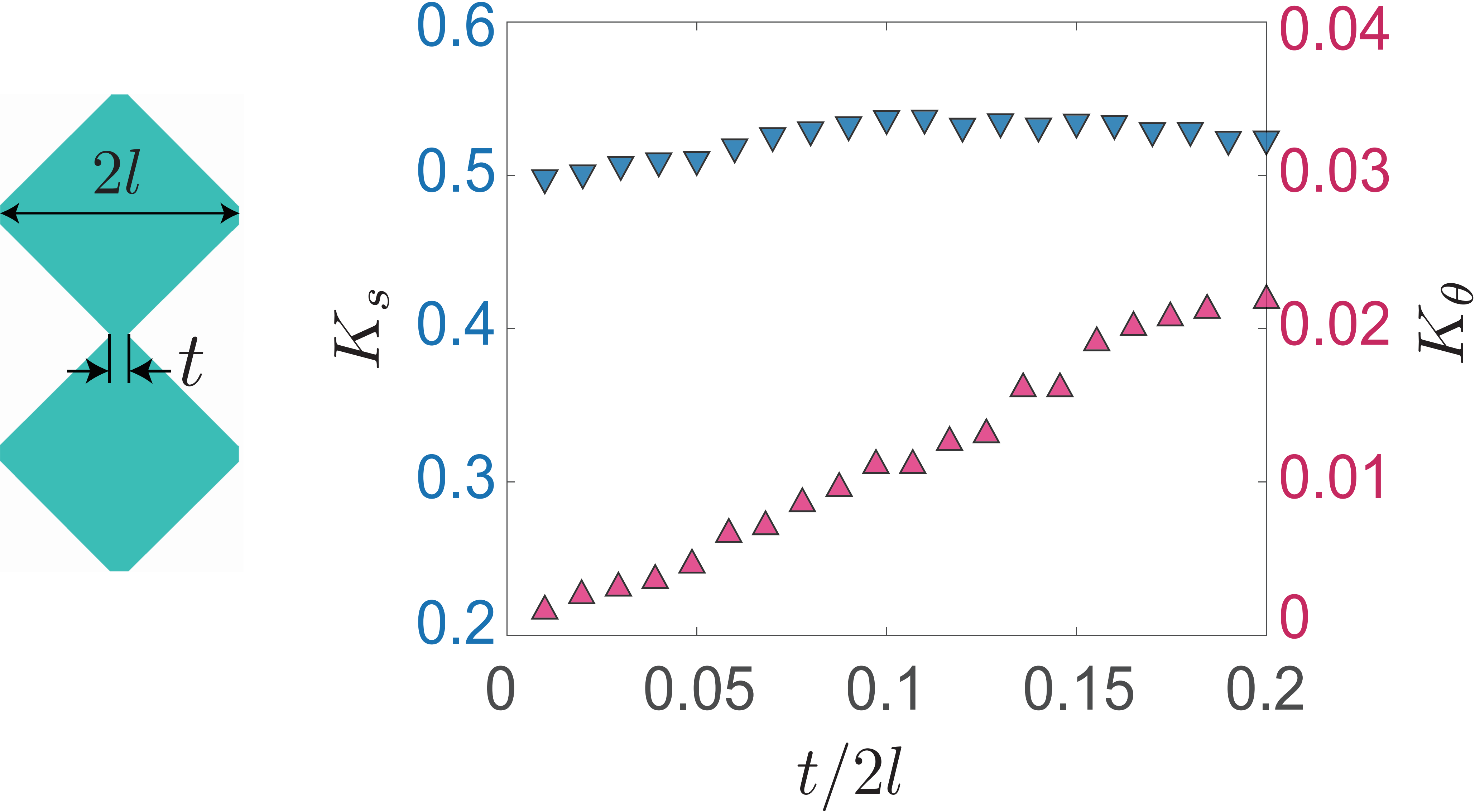

2l
t
0.6
0.5
0.4
0.3
0.2
K_s
0.04
0.03
0.02
0.01
0
K_θ
0
0.05
0.1
0.15
0.2
t/2l

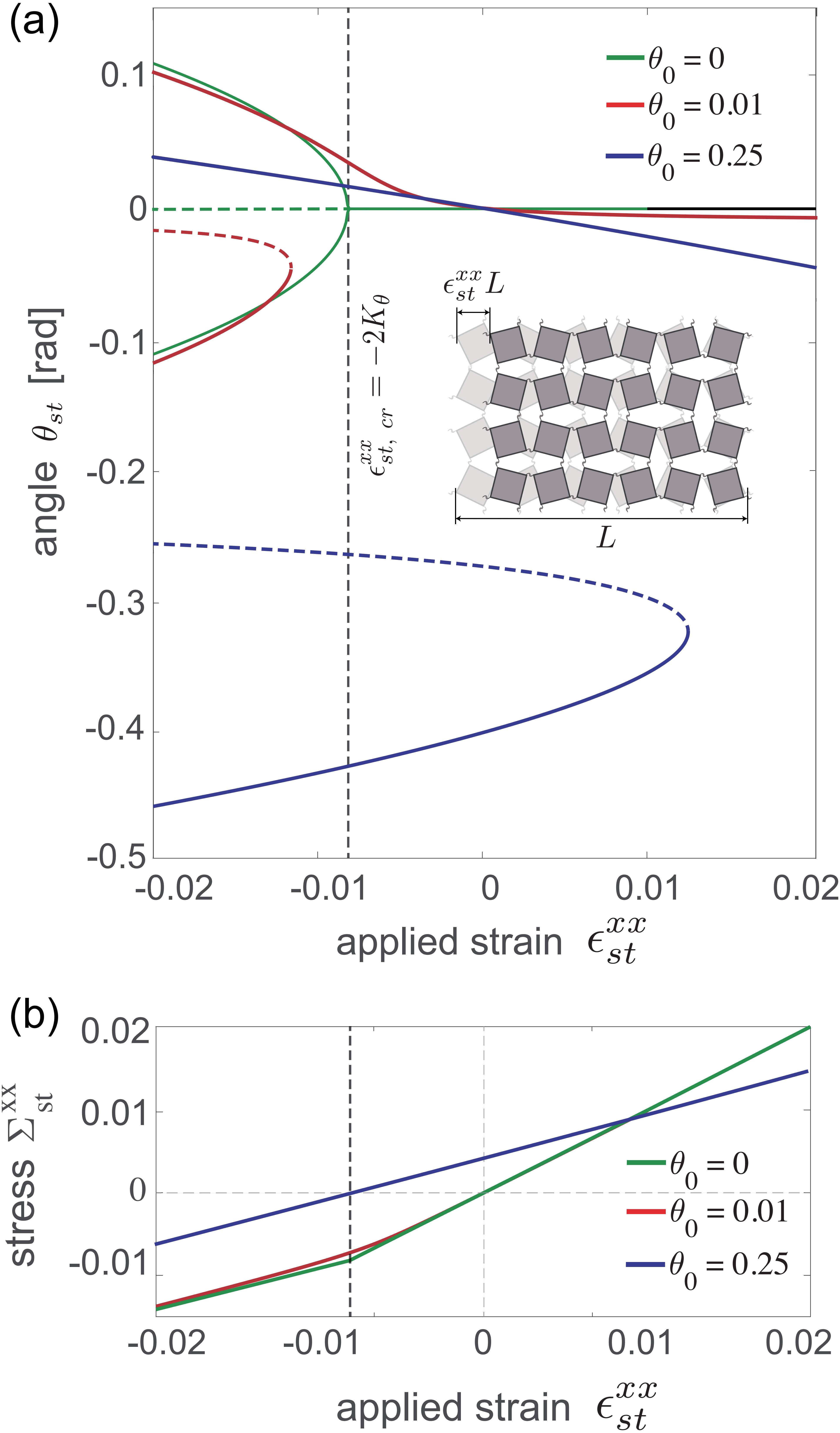

(a)
$\theta_0 = 0$
$\theta_0 = 0.01$
$\theta_0 = 0.25$
angle θ_{st} [rad]
$\epsilon^{xx}_{st,\ cr} = -2K_\theta$
$\epsilon^{xx}_{st} L$
L
applied strain ϵ^{xx}_{st}
(b)
stress $\Sigma^{\mathrm{xx}}_{\mathrm{st}}$
$\theta_0 = 0$
$\theta_0 = 0.01$
$\theta_0 = 0.25$
applied strain ϵ^{xx}_{st}

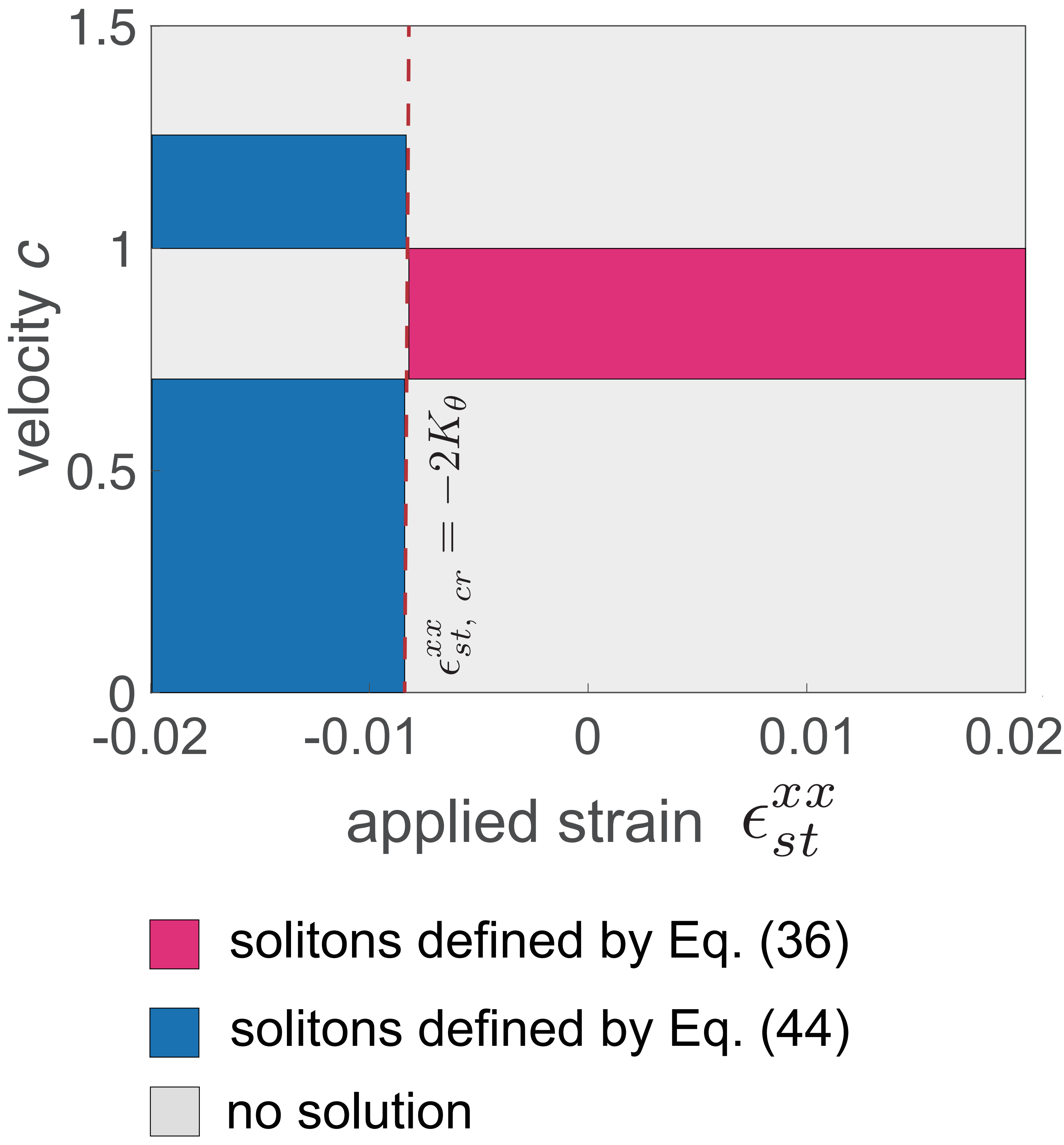

1.5
1
0.5
0
velocity c
$\epsilon_{st,\ cr}^{xx} = -2K_\theta$
-0.02
-0.01
0
0.01
0.02
applied strain ϵ_{st}^{xx}
solitons defined by Eq. (36)
solitons defined by Eq. (44)
no solution

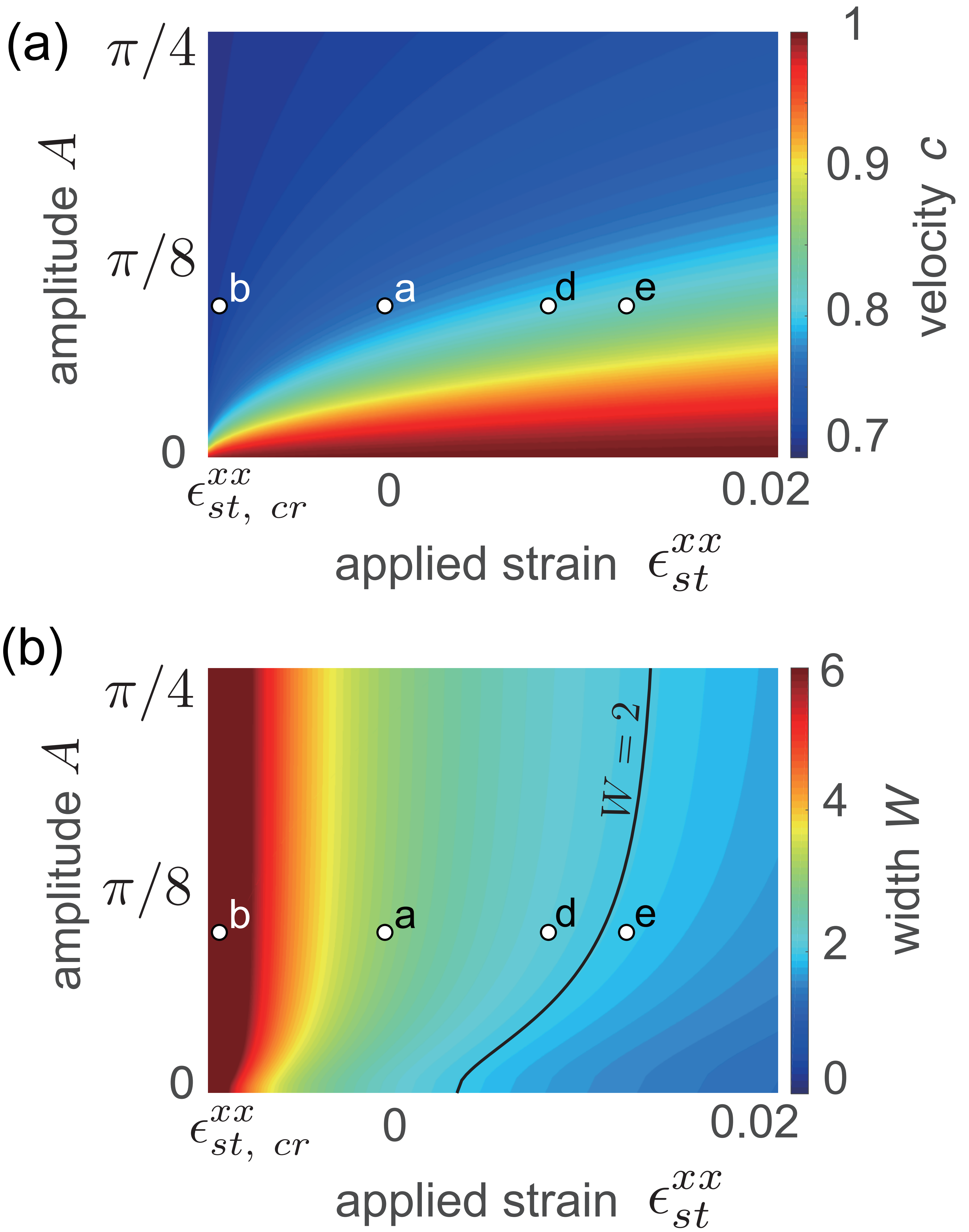

(a)
$\pi/4$
$\pi/8$
0
amplitude A
b
a
d
e
$\epsilon^{xx}_{st,\ cr}$
0
0.02
applied strain ϵ^{xx}_{st}
1
0.9
0.8
0.7
velocity c
(b)
$\pi/4$
$\pi/8$
0
amplitude A
$W=2$
b
a
d
e
$\epsilon^{xx}_{st,\ cr}$
0
0.02
applied strain ϵ^{xx}_{st}
6
4
2
0
width W


(a)
$\epsilon_{st}^{xx} = 0$
angle $\theta^{[i,j]}$ [rad]
discrete
continumn
unit number i
displacement $U^{[i,j]}$
(b)
$\epsilon_{st}^{xx} = -0.008$
(c)
$\epsilon_{st}^{xx} = -0.018$
(d)
$\epsilon_{st}^{xx} = 0.008$
(e)
$\epsilon_{st}^{xx} = 0.012$
(f)
amplitude A
$\pi/8$
$W = 2$
$N_{0.5A}$
1000
100
10
$\epsilon_{st,\ cr}^{xx}$
0.02
applied strain ϵ_{st}^{xx}

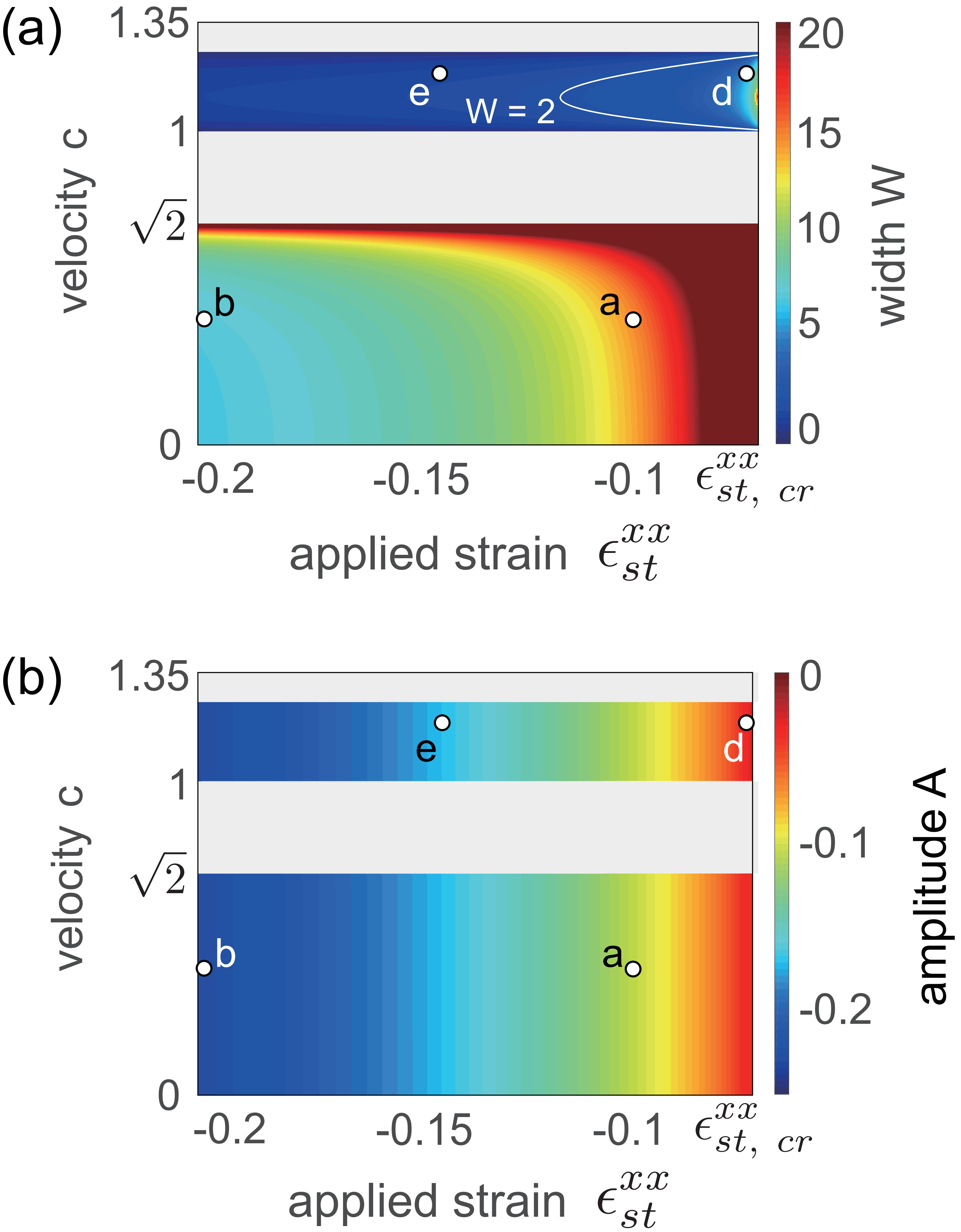

(a)
1.35
1
$\sqrt{2}$
0
velocity c
e
d
W = 2
b
a
-0.2
-0.15
-0.1
$\epsilon^{xx}_{st,\ cr}$
applied strain ϵ^{xx}_{st}
20
15
10
5
0
width W
(b)
1.35
1
$\sqrt{2}$
0
velocity c
e
d
b
a
-0.2
-0.15
-0.1
$\epsilon^{xx}_{st,\ cr}$
applied strain ϵ^{xx}_{st}
0
-0.1
-0.2
amplitude A

(a)
$\epsilon_{st}^{xx} = -0.01,\ c = 0.4$
discrete
continumn
angle $\theta^{[i,j]}$ [rad]
displacement $U^{[i,j]}$
unit number i
(b)
$\epsilon_{st}^{xx} = -0.02,\ c = 0.4$
angle $\theta^{[i,j]}$ [rad]
displacement $U^{[i,j]}$
unit number i
(c)
$\epsilon_{st}^{xx} = -0.02,\ c = 0.4$
angle $\theta^{[i,j]}$ [rad]
displacement $U^{[i,j]}$
unit number i
(d)
$\epsilon_{st}^{xx} = -0.0085,\ c = 1.2$
angle $\theta^{[i,j]}$ [rad]
$\times 10^{-3}$
displacement $U^{[i,j]}$
unit number i
(e)
$\epsilon_{st}^{xx} = -0.015,\ c = 1.2$
$\epsilon_{st}^{xx} = -0.015,\ c = 1.2$
angle $\theta^{[i,j]}$ [rad]
displacement $U^{[i,j]}$
unit number i

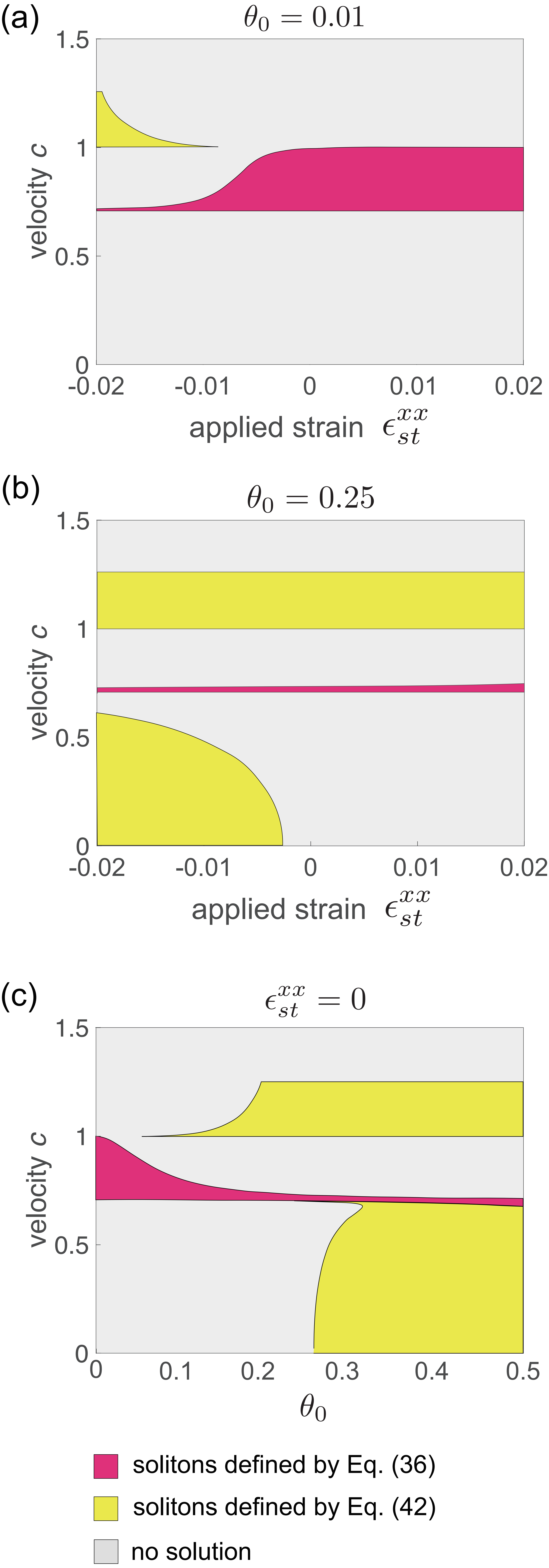

(a)
$\theta_0 = 0.01$
1.5
1
0.5
0
velocity c
-0.02
-0.01
0
0.01
0.02
applied strain ϵ_{st}^{xx}
(b)
$\theta_0 = 0.25$
1.5
1
0.5
0
velocity c
-0.02
-0.01
0
0.01
0.02
applied strain ϵ_{st}^{xx}
(c)
$\epsilon_{st}^{xx} = 0$
1.5
1
0.5
0
velocity c
0
0.1
0.2
0.3
0.4
0.5
θ_0
solitons defined by Eq. (36)
solitons defined by Eq. (42)
no solution

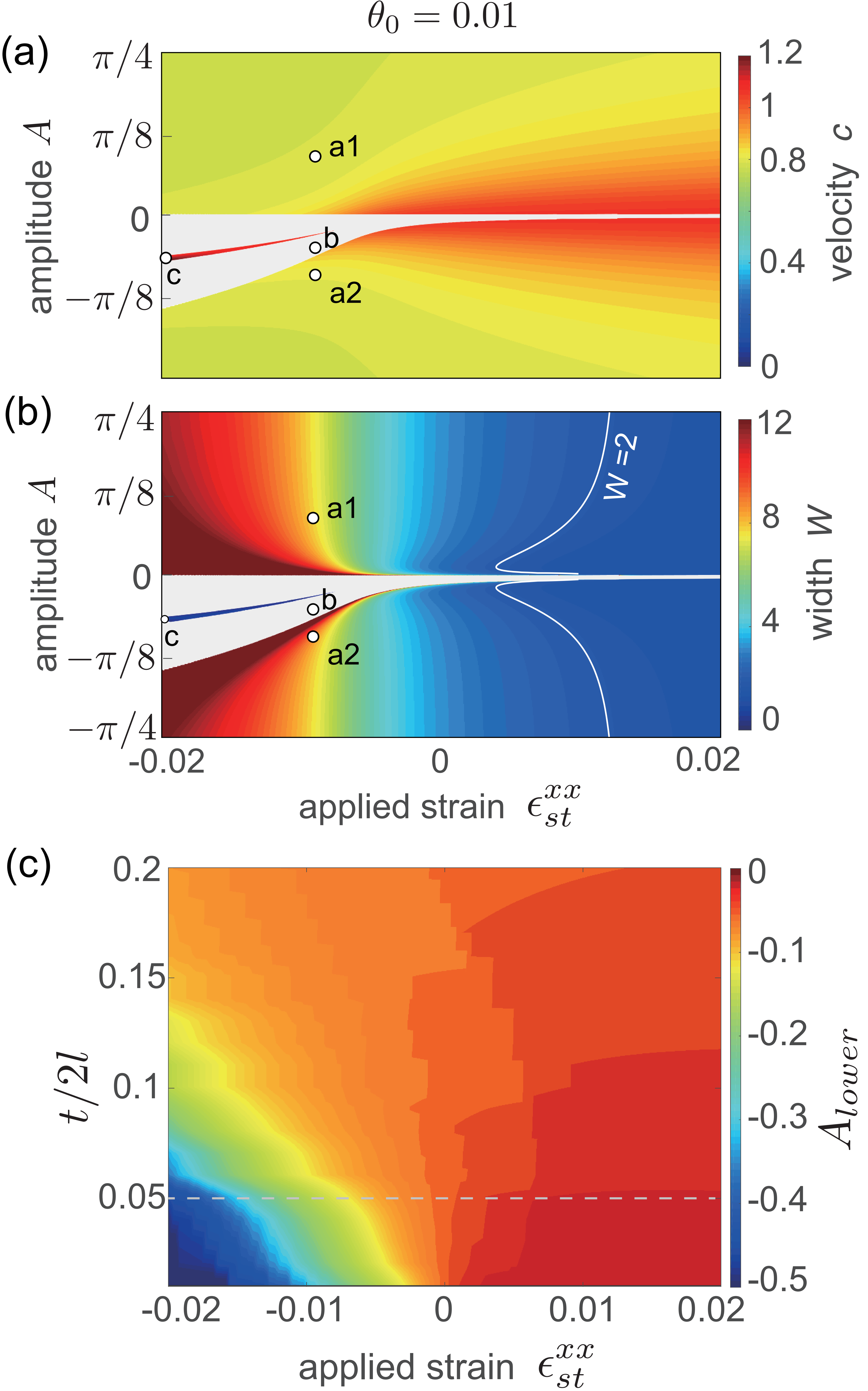

$\theta_0 = 0.01$
(a)
amplitude A
$\pi/4$
$\pi/8$
0
$-\pi/8$
a1
b
c
a2
velocity c
1.2
1
0.8
0.4
0
(b)
amplitude A
$\pi/4$
$\pi/8$
0
$-\pi/8$
$-\pi/4$
a1
b
c
a2
$W=2$
width W
12
8
4
0
-0.02
0
0.02
applied strain ϵ_{st}^{xx}
(c)
$t/2l$
0.2
0.15
0.1
0.05
A_{lower}
0
-0.1
-0.2
-0.3
-0.4
-0.5
-0.02
-0.01
0
0.01
0.02
applied strain ϵ_{st}^{xx}

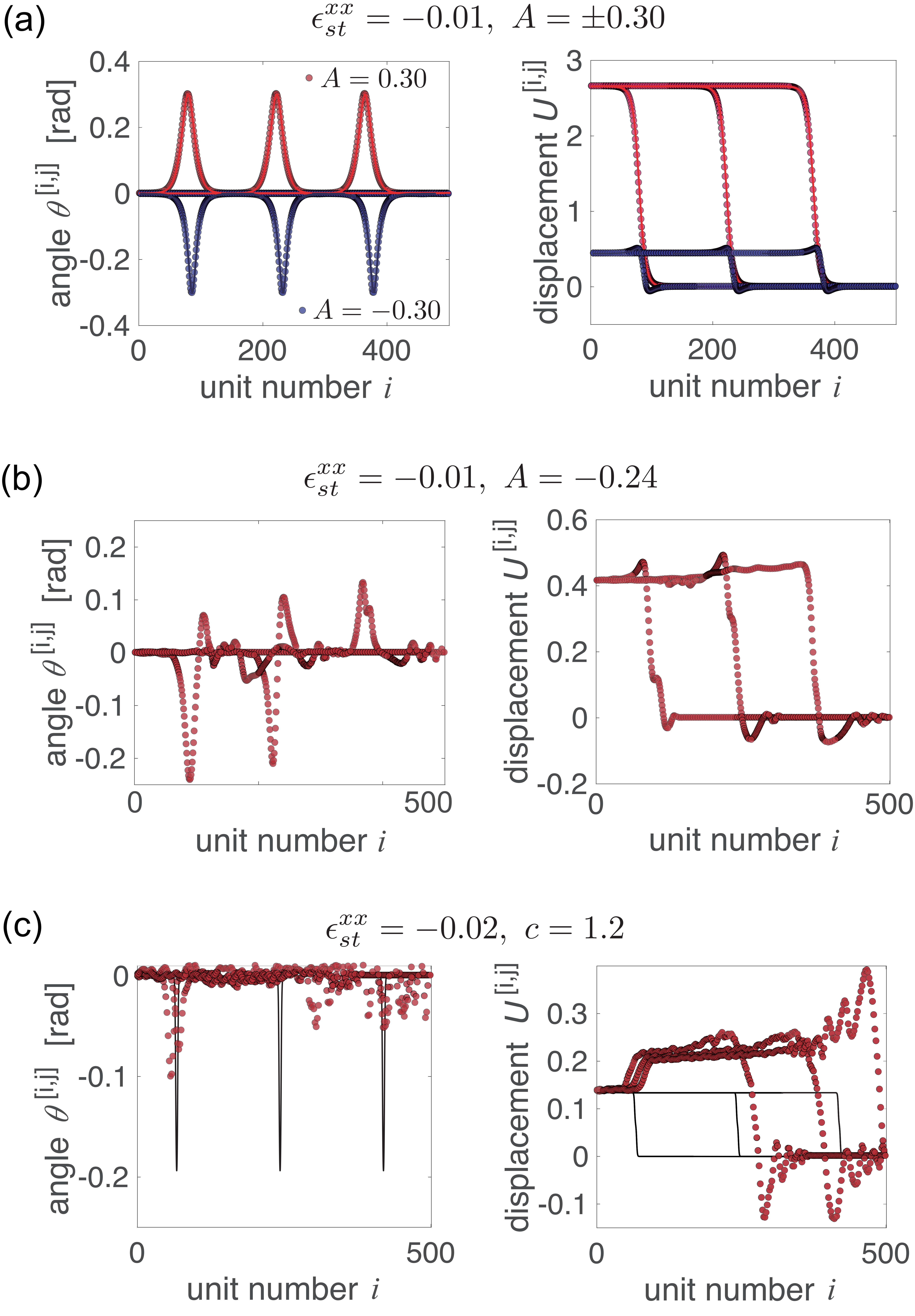

(a)
$\epsilon_{st}^{xx} = -0.01,\ A = \pm 0.30$
angle $\theta^{[i,j]}$ [rad]
$A = 0.30$
$A = -0.30$
unit number i
displacement $U^{[i,j]}$
unit number i
(b)
$\epsilon_{st}^{xx} = -0.01,\ A = -0.24$
angle $\theta^{[i,j]}$ [rad]
unit number i
displacement $U^{[i,j]}$
unit number i
(c)
$\epsilon_{st}^{xx} = -0.02,\ c = 1.2$
angle $\theta^{[i,j]}$ [rad]
unit number i
displacement $U^{[i,j]}$
unit number i

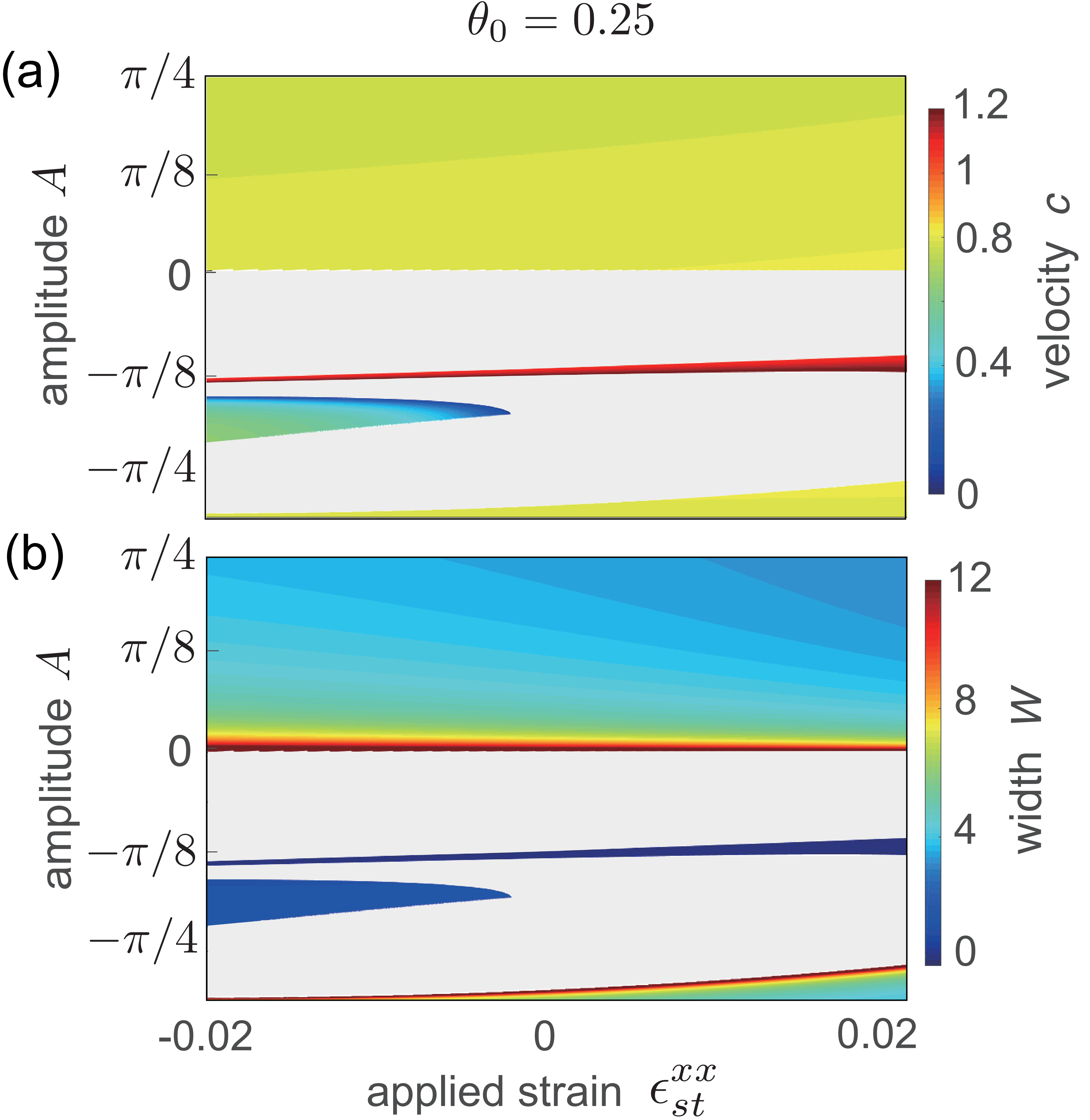

$\theta_0 = 0.25$
(a)
(b)
$\pi/4$
$\pi/8$
0
$-\pi/8$
$-\pi/4$
amplitude A
velocity c
1.2
1
0.8
0.4
0
width W
12
8
4
0
-0.02
0
0.02
applied strain ϵ_{st}^{xx}

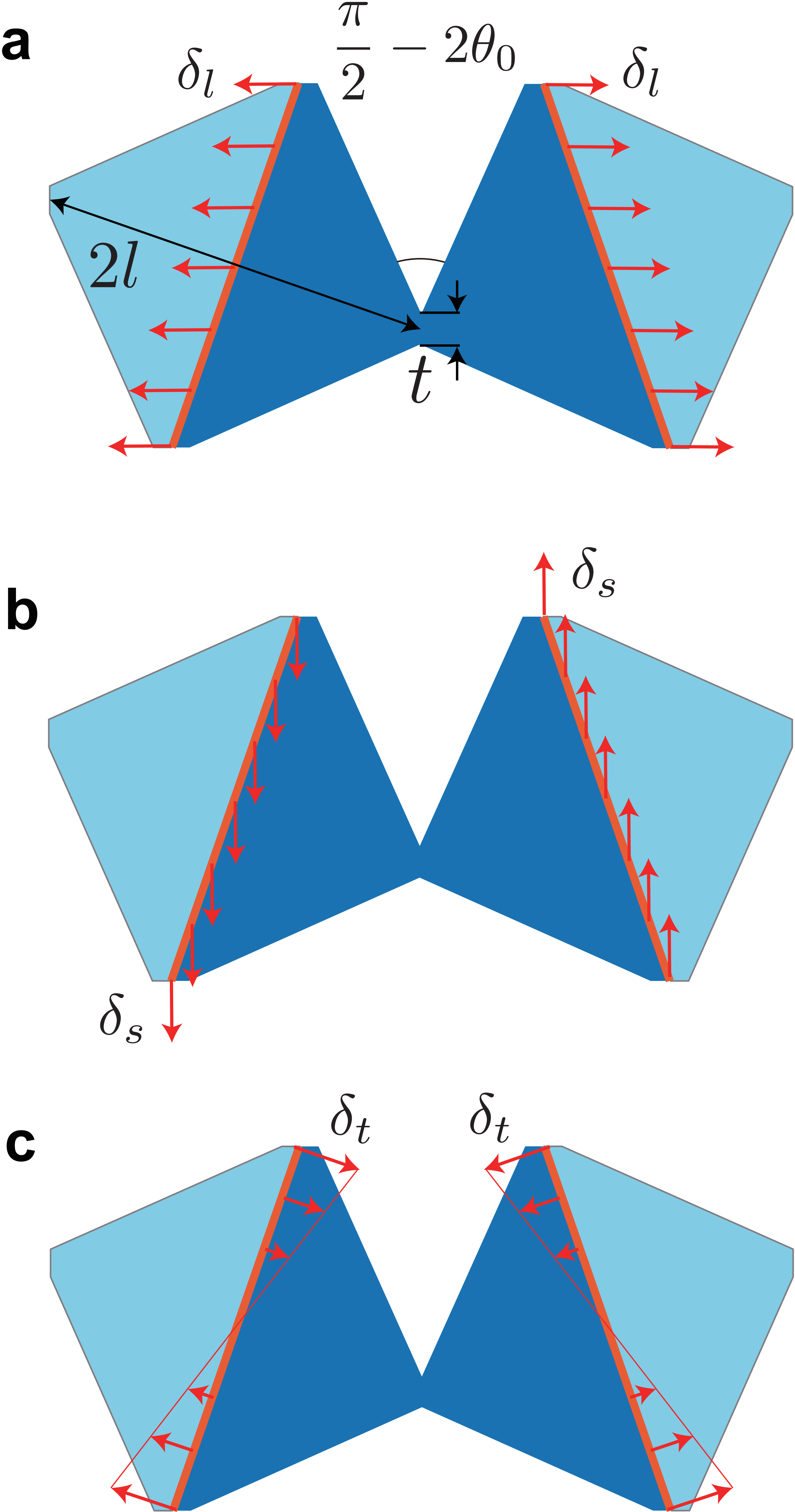

a
δ_l
$\frac{\pi}{2} - 2\theta_0$
δ_l
$2l$
t
b
δ_s
δ_s
c
δ_t
δ_t